

# ON THE EVOLUTION OF THE CRYSTALLINE STRUCTURE OF CATFISH OTOLITHS

by

R.W. GAULDIE, A. KELLERMANN\*, R. RADTKE AND S. SHARMA (1)

**ABSTRACT.** - The otoliths (sagitta, astericus, and lapillus) of the channel catfish (*Ictalurus punctatus*), the walking catfish (*Clarias fuscus*) and the loricated catfish (*Hypostomus* sp.) were examined for calcium carbonate polymorphism and crystalline morphology. Calcium carbonate polymorphisms were determined by Raman spectroscopy, and crystalline structure was observed directly using scanning electron microscopy. In the three catfish species all of the otoliths were aragonitic, but showed a trend towards decreasing crystal size from *I. punctatus*, through *C. fuscus* to *Hypostomus* sp. Combinations of twinning and selective inhibition of the growth of certain crystal faces, have resulted in crystalline habits ranging from pseudo-cuboidal to amorphous. In addition to catfish otoliths, the otolith (sagitta) of one of the most primitive Ostariophysine fish, *Goniorhynchus goniorhynchus* was described. It is proposed that the variation in otolith shape can be regarded as allometric, resulting from the effects of species-specific regulatory genes on order-specific structural genes.

**RÉSUMÉ.** - Les otolithes (sagitta, astericus et lapillus) des poissons-chats, *Ictalurus punctatus*, *Clarias fuscus* et *Hypostomus* sp. ont été examinés pour le polymorphisme du carbonate de calcium et la morphologie cristalline. Les polymorphismes du carbonate de calcium ont été déterminés par spectrophotométrie de Raman et les structures cristallines ont été observées directement en utilisant un microscope électronique à balayage. Dans les trois espèces de poissons-chats, tout les otolithes étaient aragonitiques, mais la taille des cristaux a tendance à décroître de *I. punctatus* à *Hypostomus* sp. en passant par *C. fuscus*. Les combinaisons entre la torsion et l'inhibition sélective de la croissance de certaines faces des cristaux ont donné des constitutions cristallines différentes, de pseudo cuboïdales jusqu'à des formes amorphes. De plus, l'otolithe (sagitta) de l'un des Ostariophysaires les plus primitifs, *Goniorhynchus goniorhynchus*, est décrit. Les variations dans la forme des otolithes pourraient être considérées comme allométriques, résultant des effets de gènes régulateurs spécifiques de l'espèce sur des gènes structuraux spécifiques de l'ordre.

**Key-words.** - Siluriformes, *Ictalurus punctatus*, *Clarias fuscus*, *Hypostomus* sp., Calcium carbonate polymorphism, Crystalline structure, SEM, Otoliths.

Most teleosts have three otoliths in each of the paired endolymphatic sacs of the inner ear. Teleost otoliths are composed of calcium carbonate, usually in the twinned aragonite form (Gauldie and Nelson, 1988), invested with a protein matrix (Degens *et al.*, 1969; Zhang, 1992) and are mechanical sound transducers (Fay, 1984). The three otoliths usually have a species-specific shape (Gaemers, 1984), although otoliths with irregular shapes that are sometimes composed of other morphs of calcium carbonate (calcite, vaterite) also occur (Strong *et al.*, 1986; Gauldie, 1986). In most teleosts the largest otolith, the sagitta, occupies the endolymphatic sac, with a smaller otolith, the astericus, in a diverticulum off the endolymphatic sac. The smallest of the three otoliths, the lapillus, is usually found in the atrium of the semi-circular canals (Dale, 1976). The

(1) Hawaii Institute of Geophysics, School of Ocean and Earth Science and Technology, University of Hawaii, 2525 Correa Road, Honolulu, HI 96822, USA.

\* Present address: Nationalparkamt Wattenmeer, Schloßgarten 1, D 2254 Tönning, GERMANY.

otoliths of teleost fishes have been widely used in the systematics of both fossil (Nolf, 1985; Schultze, 1990) and recent (Gaemers, 1984) fishes, usually based on the similarities in gross morphology of otoliths of closely related species.

The Siluriformes (Ostariophysii) are characterized by a modified swim-bladder that is connected mechanically to the inner ear via a chain of bony structures called the weberian ossicles. The anatomy of the weberian ossicles in relation to both the swim-bladder and the endolymphatic sac of the inner ear has been described for the major families of catfishes by Chardon (1968). In catfishes the relative sizes of the three otoliths of the endolymphatic sac are quite different from other fishes. In most catfishes the lapillus and astericus are larger (heavier) than the sagitta, rather than smaller as in most teleosts; and in some catfishes (e.g. *Selenaspis herzbergii*) the lapillus is enormously enlarged, up to 5 times longer than the sagitta (Chardon, 1968). The differences in size of otoliths are reflected in the organisation of maculae, otolithic membranes and the endolymphatic ducts of the catfish inner ear (Jenkins, 1977; 1979).

In addition to the changes in relative size, the otoliths of some catfishes have a different crystalline morphology from those of other teleosts. The structure of otoliths from some species of catfish are known to have a coarsely crystalline structure, that makes them unsuitable for fish aging techniques based on the conventional patterns of internal opaque and hyaline zones or check rings (Appelgate and Smith, 1951; Dean *et al.*, 1983). In this paper we explore the crystalline structure of otoliths of the catfishes *Ictalurus punctatus* (the channel catfish), *Clarias fuscus* (the walking catfish) and *Hypostomus* sp. (the loricated catfish) with optical and scanning electron microscopy as well as Raman resonance spectroscopy. In addition, we have examined the crystalline structure of the sagitta of the marine sand eel, *Gonorrhynchus gonorrhynchus* that is regarded as the most primitive of extant Ostariophysine fishes (Fink and Fink, 1987). Our aims are to assess the qualitative and quantitative variations in crystal morphology that have progressively changed between otoliths during the course of evolution of different species of catfishes.

## MATERIALS AND METHODS

Specimens of *Ictalurus punctatus*, *Clarias fuscus* and *Hypostomus* sp. were obtained from water reservoirs on the island of Oahu, Hawaii. All fish were killed by freezing after quinaldine anesthesia and the three otoliths dissected out from each endolymphatic sac. After washing in distilled water and air-drying, some otoliths were fixed to stainless steel pin stubs with colloidal silver paint and photographed by scanning electron microscopy (SEM).

Raman techniques for calcium carbonate mineral identification were used following the procedures described by Sharma (1989) and Urmos *et al.* (1991). Aragonite and calcite can be distinguished by different peaks in their Raman spectra. For example in their study of biogenic carbonates Urmos *et al.* (1991) showed Raman spectra typical of aragonite in natural and cultured pearls, the scleractinian coral *Porites* sp. as well as from synthetic aragonite. Conversely, Raman spectra typical of calcite were recovered from pink and white precious corals (*Corallium regale* and *C. secundum* respectively) as well as synthetic magnesian calcite and geological calcite. Raman spectra arise from the same lattice organization effects that result in the well-known x-ray diffraction spectra of minerals (Bischoff *et al.*, 1985). Raman spectra provide a very reliable and convenient tool for assigning mineral species. As an example, the Raman scattering spectra of the sulcal side of the channel catfish sagitta is shown as intensity (counts) plotted against Raman shift which is expressed as the inverse of wavelength (Fig. 1). The primary peak at  $1087\text{ cm}^{-1}$  identifies the chemistry of the mineral as calcium carbonate, and the harmonics at  $707\text{ cm}^{-1}$ ,  $256\text{ cm}^{-1}$  and  $221\text{ cm}^{-1}$  identify the lattice organization as consistent with aragonite.

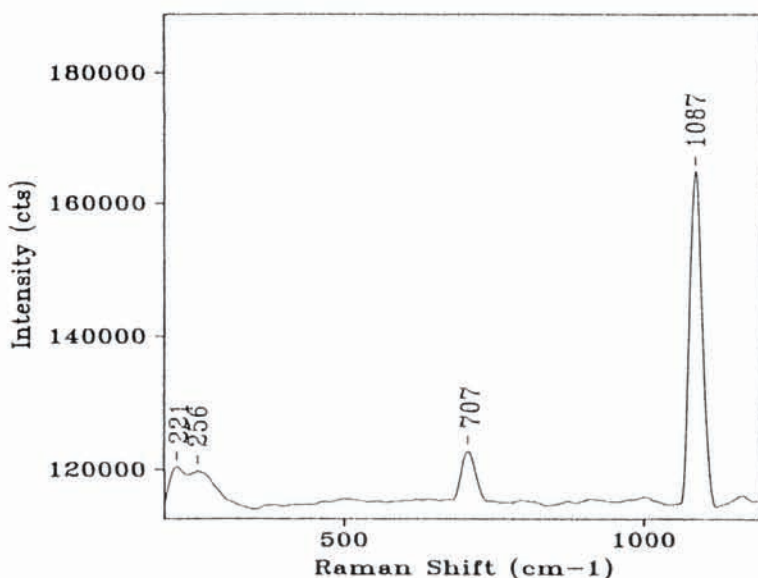


Fig. 1. - The Raman spectra of the sulcal side of aragonite from the sagitta of *Ictalurus punctatus* is shown as intensity (counts) plotted against Raman shift expressed as wavenumber ( $\text{cm}^{-1}$ ). The wavenumbers of the spectral lines are indicated on the graph.

The otoliths of the channel catfishes are oriented *in situ* so that the medial planes of the sagitta and astericus are roughly  $90^\circ$  out of phase with the medial plane of the lapillus. The usual description of otolith orientation is in terms of the sulcus (macula-adjointing) face being "inward facing" and the anti-sulcus face being "outward facing" (Panella, 1980). This description of orientation is not appropriate for catfish otoliths because of the differences in orientation among otoliths. Instead, we describe orientation arbitrarily in terms of the isolated otolith lying sulcus side (i.e. macula-adjointing side) down on a flat surface, thereby defining the sulcal and anti-sulcal side of the otolith. A similar convention is followed in Gauldie *et al.* (1991). Anterior and posterior parts of the otolith are described as such, but it is necessary to refer to the right-hand and left-hand sides of the lapillus instead of ventral and dorsal as is the case with sagitta and astericus. Right and left are taken in the sense of facing the same direction as the fish. These conventions will be more readily appreciated by examining the respective figures later in the text. The orientation of crystals within otoliths are described as horizontal when it is in or near, the same plane as the macula, and vertical when orthogonal to the plane of the macula.

Calcium carbonate crystals show different habits, as well as different kinds of mineral polymorphisms. Habit is the crystallographic term used to describe those variations in crystal form that occur within a particular crystal polymorphism (Bloss, 1971). Within a single species of fish calcium carbonate hard parts may show a very wide variation in habit leading to a large number of crystals with distinctive shapes that are stable at standard temperature and pressure. The nomenclature of some of the habits of calcium carbonates follows that of Carriker *et al.* (1980).

The quantitative approach to assessing variation in the crystal structure within characteristic habits of otoliths depends on measurements of the basic structural order associated with the growth of the crystal. Growth can be structurally described in terms of the kinks in the steps on the crystal surface that have been formed by the lamellae of the growing crystal (Fig. 2a). When kinks reach the end of the steps in the crystal formed

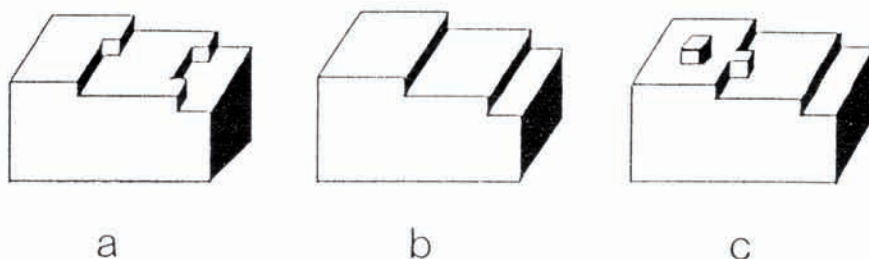


Fig. 2. - a) Kinks (arrows) form at the edges of the steps (open arrows) that form the lamellae of the crystal. b) As kinks fill in, the steps (open arrows) on the growing crystal form the discrete layers of the lamellae of the crystal. c) New kinks form when new growth units appear (arrows) on steps of the lamella, or appear on the surface of the lamellae (open arrows). Growth units develop on both the horizontal (H) and vertical (V) planes of the crystal resulting in lamellae growing simultaneously in the horizontal and vertical planes.

by lamellae they disappear, leaving a discrete layer or lamella (Fig. 2b). New kinks appear spontaneously at the edges of complete steps (Fig. 2c), or may appear as single growth units on the surface of the complete lamellae (Fig. 2c). Growth units develop on both the horizontal and vertical planes of the growing crystal resulting in continuous growth (albeit at different rates) in both the horizontal and vertical planes of the otolith. A more complete description of crystal surface growth is given in Nielsen and Christoffersen (1982).

Crystal habit is described as cuboidal, monoclinic, hexagonal etc. The basic crystalline form of aragonite is an orthorhombic lath but because of twinning (Bloss, 1971) orthorhombic crystals rarely appear in biominerals. Crystal location on the otolith, crystal shape, orientation and diameter are shown in table I by species. The widths of horizontal and vertical crystal lamellae, average growth unit diameter and apex morphology of crystals define much of the crystalline growth characteristics of biominerals and are shown in table I.

The sulcal side of the catfish otolith differs from most other teleost otoliths in having a number of grooves separated by what are referred to by Jenkins (1977; 1979) as inferior, median and superior flutes corresponding to the ventral, central and dorsal parts of the otolith respectively. The nomenclature of Jenkins is followed here.

## RESULTS

### The channel catfish, *Ictalurus punctatus*

The general anatomical arrangements of the inner ear and the location of the otoliths of *Ictalurus punctatus* are shown in Chardon (1968) and Jenkins (1977; 1979).

After removal of the endolymphatic sac it was possible in some individuals of *I. punctatus* to photograph the macula underlying each otolith using polarised light. The maculae of the astericus and sagitta showed well developed central nerves that reflected the shape of the sulcus (which is described below) of both otoliths as described in Jenkins (1977; 1979). The macula of the lapillus showed a much more diffuse pattern of innervation that covered most of the area of contact between the sac and the upper side of the otolith. The area of contact was rounded to match the rounded surface of the macula.

Ten specimens of channel catfish were dissected. Although there was some individual variation in the size of the single crystals observed growing on the otolith, the otoliths of the channel catfish showed a consistent pattern of shapes and relative sizes among individual fishes.

Table 1. - Crystal dimensions are listed by species, otolith and the side of the otolith (sulcal or anti-sulcal) that was examined.

| Otolith                     | Surface        | Crystal shape                  | Orientation of lateral face to macula ( $\mu\text{m}$ ) | Average crystal diameter ( $\mu\text{m}$ ) | Average horizontal lamella width ( $\mu\text{m}$ ) | Average vertical lamella width ( $\mu\text{m}$ ) | Average growth unit diameter ( $\mu\text{m}$ ) | Apex morphology | Length: width |
|-----------------------------|----------------|--------------------------------|---|--|--|--|--|-----------------|---------------|
| <i>Ictalurus punctatus</i>  | anti-sulcal    | cuboidal                       | vertical  | 500.0                                      | 1.28   | 1.5  | 0.60   | half-hexagonal  | 1:1           |
|                             | interior flute | monoclinical                   | vertical  | 10.7                                       | ---  | 0.5  | 0.50   | hexagonal       | 10:1          |
|                             | superior flute | monoclinical                   | vertical  | 11.0                                       | ---  | ---  | ---  | ---             | 35:1          |
|                             | median flute   | amorphous                      | ---   | ---  | ---  | ---  | 0.30   | ---             | ---           |
|                             | sulcal groove  | cuboidal                       | ---   | 56.0                                       | ---  | ---  | 0.80   | ---             | ---           |
|                             | sulcal groove  | hexagonal                      | parallel  | 80-100                                     | ---  | ---  | ---  | ---             | ---           |
|                             | anti-sulcal    | ---                            | vertical; rotating to parallel at edge                  | 1000                                       | 7.00   | 8.0  | ---  | hexagonal       | 1:1           |
|                             | sulcal         | hexagonal                      | vertical; rotating to parallel at edge                  | 1000                                       | ---  | 3.1  | ---  | hexagonal       | 3:1           |
|                             | sulcal         | hexagonal                      | vertical; rotating to parallel at edge                  | 4.5  | ---  | ---  | 2.00   | nodular         | ---           |
|                             | anti-sulcal    | cuboidal and amorphous         | vertical; rotating to parallel at edge                  | 1000                                       | ---  | 1.7  | ---  | half-hexagonal  | 1:1           |
|                             | sulcal         | monoclinical                   | vertical; rotating to parallel at edge                  | 12.5                                       | ---  | 1.4  | 0.60   | hexagonal       | ---           |
|                             | ---            | rosette                        | ---   | ---  | ---  | ---  | ---  | ---             | ---           |
|                             | ---            | ---                            | ---   | ---  | ---  | ---  | ---  | ---             | ---           |
| <i>Clarias fuscus</i>       | anti-sulcal    | cuboidal                       | vertical  | 100  | ---  | ---  | ---  | ---             | ---           |
|                             | sulcal         | monoclinical                   | vertical  | 5-21                                       | ---  | ---  | ---  | ---             | ---           |
|                             | sulcal         | monoclinical to lobate at edge | vertical  | 75.0                                       | ---  | ---  | ---  | ---             | 16:1          |
|                             | anti-sulcal    | plate-like                     | ---   | 2.0  | ---  | ---  | ---  | ---             | ---           |
| <i>Hypostomus</i> sp.       | anti-sulcal    | monoclinical                   | vertical  | 25.0                                       | ---  | ---  | ---  | ---             | 50:1          |
|                             | sulcal         | monoclinical                   | vertical  | 42.0                                       | ---  | ---  | ---  | ---             | 20:1          |
|                             | anti-sulcal    | amorphous                      | horizontal  | ---  | ---  | ---  | ---  | ---             | ---           |
|                             | sulcal         | amorphous                      | vertical  | 1.25                                       | 0.75   | ---  | 0.75   | ---             | ---           |
|                             | anti-sulcal    | monoclinical                   | monoclinical  | 15.0                                       | 0.40   | ---  | 0.40   | ---             | 50:1          |
|                             | sulcal         | amorphous                      | horizontal  | 13.0                                       | ---  | ---  | ---  | ---             | 13:1          |
| <i>Gonorhynchus sagitta</i> | ---            | laths                          | horizontal  | 1.3  | ---  | ---  | 0.60   | ---             | 200:1         |
|                             | sulcal         | cuboidal                       | vertical  | ---  | 1.60   | 1.6  | 0.05   | ---             | 1:1           |

### *Sagitta*

The sagittae of *I. punctatus* had a coarse crystalline surface on the anti-sulcal side of the otolith (Fig. 3a), that gave Raman spectra typical of aragonite. The crystal structure of the anti-sulcal surface of the sagitta was organised into large cuboidal crystals. The largest crystals in figure 3a were nearly 500  $\mu\text{m}$  wide and of similar depth. The cuboidal crystals had smoother vertical (with respect to the macula sides) and coarser horizontal sides (Fig. 3a). Detail of the cuboidal structure showed steps, kinks and incipient single growth units on crystal lamellae growing in two planes (Fig. 3b).

Measurement of lamellar widths from figure 3b showed horizontal lamellae to have an average width of about 1.28  $\mu\text{m}$  ( $n = 10$ ; range 0.9-1.6) and vertical lamellae to have an average width of about 1.51  $\mu\text{m}$  ( $n = 10$ ; range 0.96-1.75). Horizontal and vertical lamellae were oriented at slightly different angles but were generally at an angle of about 90° to each other. A number of kinks were observed at the edge of the lamellae, and in some places pits were evident in the smooth crystal surface where fusion of steps was complete (Fig. 3b). In some places very narrow, parallel pits could be seen, suggesting slow coalescence of steps. A few growth units could be seen at the steps of some lamellae (Fig. 3b). Isolated growth units occur on the smooth growth surface of crystals (Fig. 3b). Viewed from another axis, the crystals still showed the signs of lamellar structure and pits associated with fusion of steps, as well as a stacked structure consisting of crystalline half-hexagons (Fig. 3c). In places growth units occurred on the half-hexagon stacks and, more uncommonly, on the vertical faces of the crystal (Fig. 3c). Growth unit diameters were generally below 1  $\mu\text{m}$  in diameter, averaging about 0.6  $\mu\text{m}$  ( $n = 10$ ; range 0.5-1.1).

The sulcal side of the sagitta showed a pair of grooves fusing to form flattened depression at the posterior end of the sagitta (Fig. 4a). The grooves were formed by the inferior, median and superior flutes. A large crystal on the anti-sulcal surface could also be seen on the dorsal side of the sagitta (Fig. 3b). The inferior flute on the ventral side of the groove was formed by a regular array of crystals (Fig. 4b) that gave Raman spectra typical of aragonite. The regular arrays of crystal were located closer to the ventral edge becoming larger and fused together into smooth lobate structure at the edge of the groove bordering the inferior flute (Fig. 4b). Crystals nearer the edge were longer than wider (about 10:1) and were characterised by wide interstices between crystals and by a tendency towards triangular crystals with chamfered edges (Fig. 4b) that progressively changed into a more amorphous structure as the crystals grow closer together. The average width of separated crystals was about 10.7  $\mu\text{m}$  ( $n = 10$ ; range 7.8-13.6). In some crystals (Fig. 4b) vertical lamellae were about 0.5  $\mu\text{m}$  ( $n = 15$ ; range 0.3-0.8) in width. Some crystals had small crystal growth units (Fig. 4b) with about the same average diameter, 0.5  $\mu\text{m}$ , as lamellar width. Traces of sharply triangular crystals in figure 4b increase in frequency towards the anterior end of the inferior flute resulting in laterally twinned triangular crystals gradually giving way to flattened hexagons (Fig. 4c). The triangular appearance of these crystals is emphasised by chamfered edges resulting from an angled cut-off in the growth of crystal lamellae (Fig. 4c). The triangular crystals vary slightly in their apical angles but all are close to the 64° angle typical of twinned aragonite (Fig. 4c).

Detail of the median flute between the two grooves of the apparent sulcus of the sagitta showed an amorphous, smooth crystalline surface (Fig. 4d), similar to that of single crystals growing in the groove of the sulcus (Fig. 4e). The surface of the median flute and the groove on either side showed a number of very small pits and very small crystalline growth units, on their surfaces (Figs. 4d; e). Pits averaged about 0.5  $\mu\text{m}$  in diameter ( $n = 10$ ) and surface crystals were smaller, about 0.3  $\mu\text{m}$  in diameter ( $n = 10$ ). The hexagonal crystals in the groove were very flat between 80 and 100  $\mu\text{m}$  diameter with almost no growth on the lateral faces and with flattened apices (Fig. 4e). Lateral faces of the hexagonal crystals within the groove were oriented horizontal to the macula.

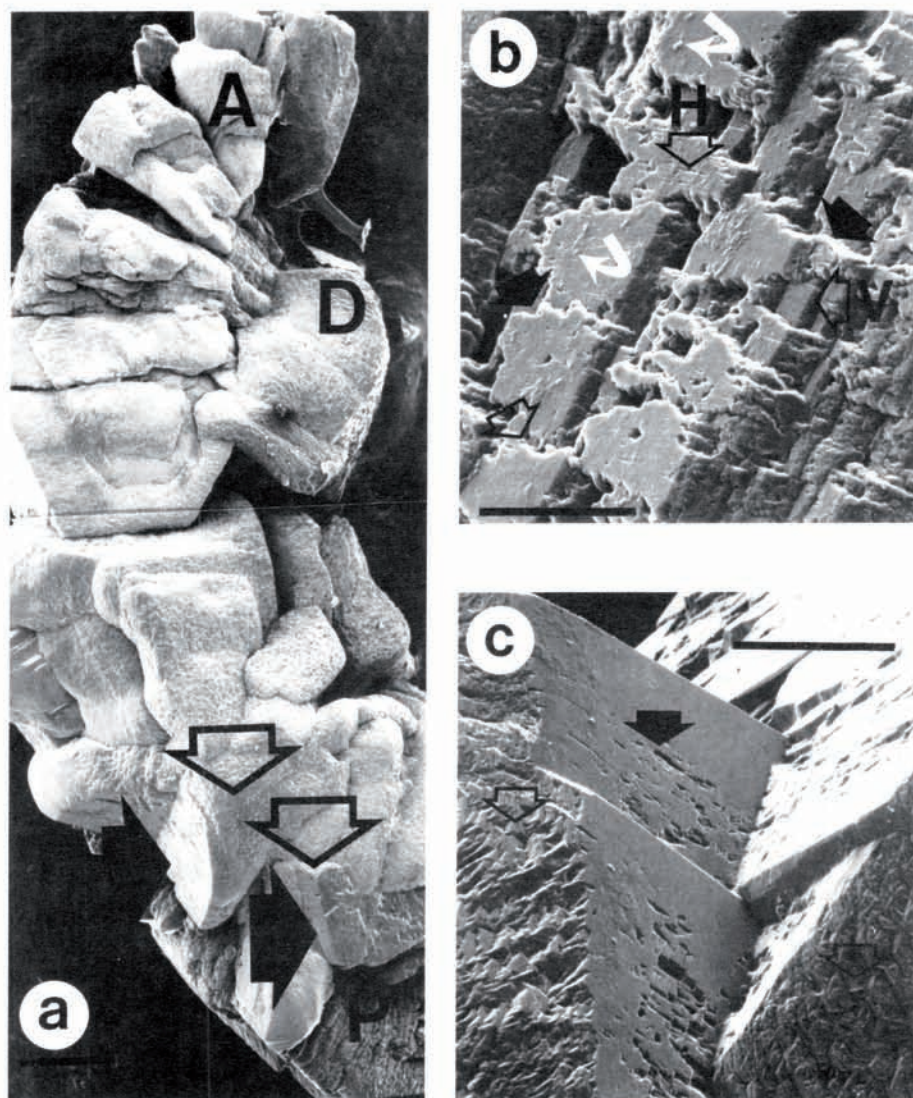
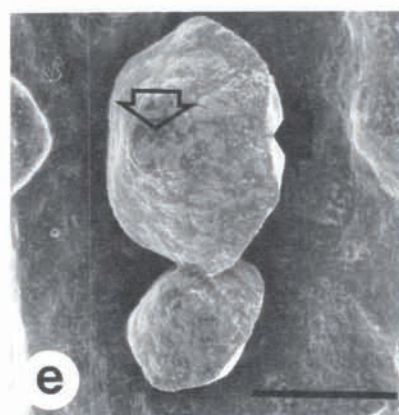
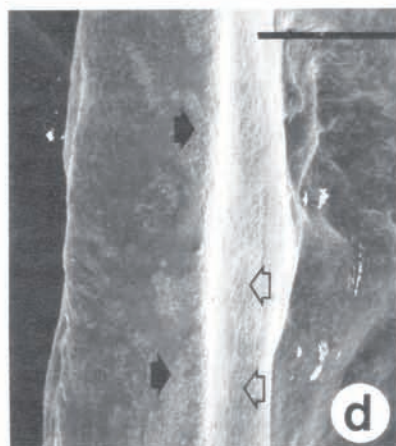
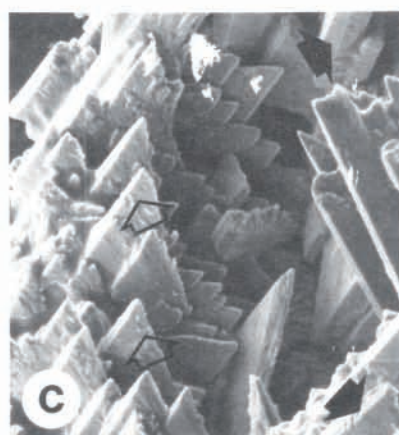
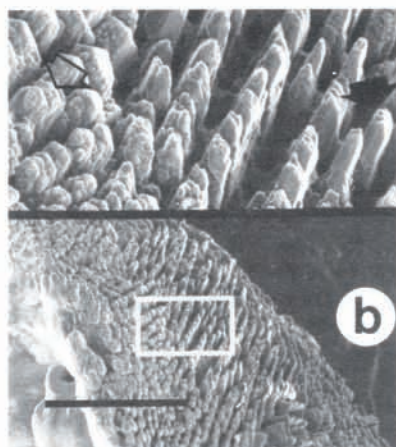
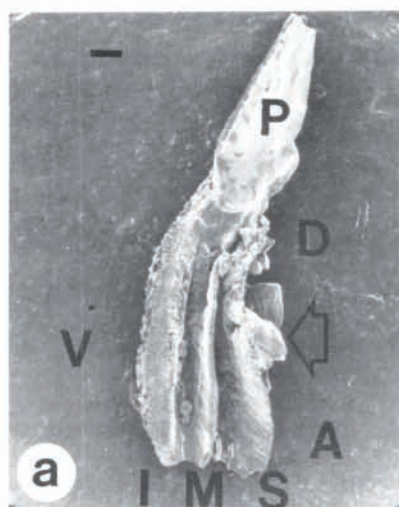


Fig. 3. - Crystalline structure of the anti-sulcal surface of the sagitta of *Ictalurus punctatus*. a) The sagitta is crescent-shaped, concave towards the dorsal (D) side. The crystals of the anti-sulcal surface are very large with a tendency to be smaller at the anterior (A) than at the posterior (P) end of the otolith. The vertical sides of the large crystals (arrows) tend to be smoother than the apices in the horizontal plane of the crystals (open arrows). Bar = 200  $\mu\text{m}$ . b) Detail of the cuboidal crystal surface shows steps (arrows) kinks (open arrow) and single growth units (curved arrows) at the steps and on the crystalline surface itself. The steps of the crystal surface indicate the variation in thickness of the horizontal lamellae (open arrow marked H) and vertical lamellae (open arrow marked V) of the crystal. Pits resulting from fusion of lamellae (outlined arrows) can be seen on the smooth crystal surface. Bar = 17.6  $\mu\text{m}$ . c) Viewed from another angle crystals of the sagitta show traces of the lamellar structure in the pits resulting from fusion of steps (arrows), but on the horizontal face of the crystal stacked half-hexagons (open arrows) appeared. Bar = 60  $\mu\text{m}$ .



The superior flute of the sulcus showed an array of long, thin crystals that abruptly changed to cuboidal crystals (average width  $56\text{ }\mu\text{m}$ ) in the floor of the groove between the superior and median flutes (Fig. 4f). Crystals at the edge of the superior flute were longer than wider (about 35:1) with an average width about  $11\text{ }\mu\text{m}$  ( $n = 27$ ). Crystals growing on the smooth surface of the groove were very small, about  $0.8\text{ }\mu\text{m}$  in diameter ( $n = 10$ ). The crystals of the central flute and the similarly surfaced hexagonal crystals in the sulcal groove, as well as both the cuboidal and monoclinic crystals of the ventral groove of the sulcus, gave Raman spectra typical of aragonite.

#### *Astericus*

The astericus of *I. punctatus* had a smooth anti-sulcal surface at the focus, becoming progressively more crystalline with crystals apparently radiating from the central focus in a roughly circular pattern (Fig. 5a). The crystals of the anti-sulcal surface of the astericus gave Raman scattering spectra typical of aragonite. The crystals of the astericus become progressively larger towards the edge of the otolith and show indications of the hexagonal habit at several stages of completion (Fig. 5a). Towards the edge of the otolith individual crystals were very large, up to 1 mm in length.

Detail of one of the single crystals on the anti-sulcal surface of the astericus showed steps, kinks and incipient single growth units of what appeared to be a single large hexagonal crystal (Fig. 5b). This single large crystal showed more narrow lamellae in the width plane of the crystal than in the length plane of the crystal (Fig. 5b). The width plane is vertical to the macula and the length plane is horizontal to the macula. Although difficult to detect clearly the average width of horizontal lamellae was about  $7\text{ }\mu\text{m}$  ( $n = 8$ ; range 0.5-0.8) and the average width of vertical lamellae was about  $8\text{ }\mu\text{m}$  ( $n = 5$ ; range 0.7-1.0). This crystal also showed co-planarity of the surfaces of the separate growth stacks forming the crystal (Fig. 5b). Co-planarity gives the impression that the crystal has been eroded.

The sulcal surface of the astericus was coarsely crystalline, with a deep central groove (Fig. 5c) that corresponded to the shape and position of the macula, but was partly encircled by a horseshoe shaped arrangement of coarse blocks of monoclinic crystals (Fig. 5c) ranging in size up to as large as those on the anti-sulcal surface. The crystals of

---

Fig. 4. - a) The sulcal surface of the sagitta has a flattened posterior (P) segment but has a fluted organisation in the anterior (A) part of the otolith with the superior (S) and medial (M) flutes flaring towards the dorsal (D) edge and a wider inferior flute (I) at the ventral (V) edge. Large crystals of the anti-sulcal surface can be seen (arrow) at the dorsal edge. Bar =  $250\text{ }\mu\text{m}$ . b) Detail of the inferior flute of the sulcal surface of the sagitta shows a regular array of crystals along the vertical edge consolidating into rounded, and then massive smooth-surfaced crystals within the grooves between the inferior and medial flute. At higher magnification separated crystals show traces of hexagonal structure (arrows) progressively changing to an amorphous structure (open arrows) as the crystals grow closer to the sulcus and changing to a triangular crystal towards the anterior end of the inferior flute. Bar =  $200\text{ }\mu\text{m}$ . c) Detail of the triangular crystals of the anterior of the inferior flute shows the progressive development of hexagonal laths (arrows). The right-hand side facing aspect of the triangular crystals shows chamfered edges resulting from incomplete growth of the crystal lamellae (open arrows). Twinning on the lateral (viewer-facing) face of the crystal is evident. Triangular crystals showed close correspondence to the approximately  $64^\circ$  twinning angle of aragonite (intersecting lines). Bar =  $25\text{ }\mu\text{m}$ . d) Detail of the surface of the medial flute of the sulcal surface of the sagitta shows a smooth surface with some very small crystals (arrow), and pits (open arrow). Bar =  $60\text{ }\mu\text{m}$ . e) Laying in the groove between the ventral and medial flutes of the sulcal surface of the sagitta are two crystals in the form of flattened hexagons, but with the same smooth surface formed from very small surface crystals as that of the central flute. The hexagons show little growth at the lateral faces (arrow) and flattened apices (open arrow). Bar =  $86\text{ }\mu\text{m}$ . f) The dorsal flute of the sulcal surface of the sagitta changes from long crystals to shorter, rounded crystals in the groove between the medial and dorsal flutes. Within the groove (lower frame) the crystal surface is smooth with very small crystals (arrow) growing on the surface. Bar =  $300\text{ }\mu\text{m}$ .

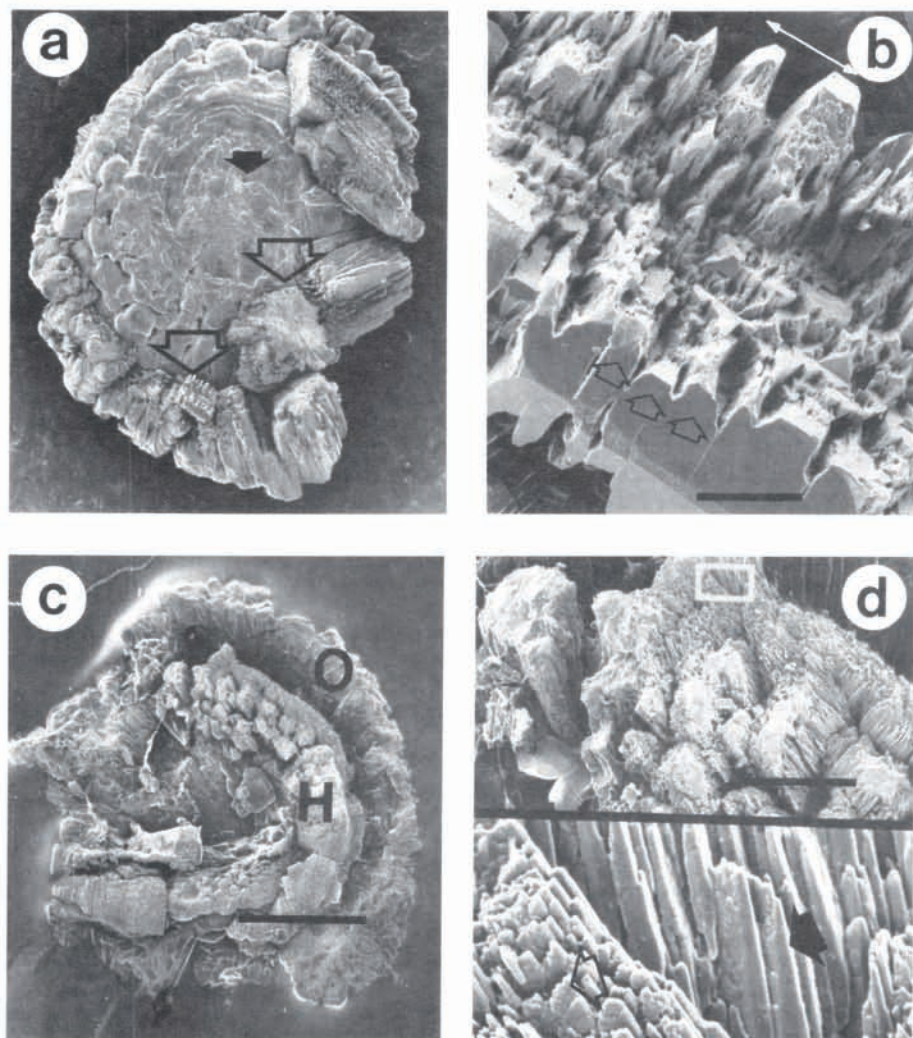


Fig. 5. - Crystalline structure of the anti-sulcal and sulcal surfaces of the astericus of *Ictalurus punctatus*. a) The anti-sulcal surface of the astericus grows in a series of concentric layers from the focus (black arrow) that become progressively thicker and more crystalline, eventually forming massive crystal blocks at the periphery of the otolith. Some of the block-like crystals show a tendency to form hexagonal crystals (open arrows) oriented both horizontally and vertically to the plane of the otolith. Bar = 250  $\mu\text{m}$ . b) Detail of one of the hexagonal crystals from (a) shows a stepped structure of vertical lamellae (arrows) parallel to the long axis of the crystal, and wider horizontal lamellae (open arrows) orthogonal to the long axis of the crystal. Growth stacks (outlined arrows) show coplanarity. Bar = 50  $\mu\text{m}$ . c) The sulcal surface of the astericus shows a horseshoe shaped inner, crystalline layer (H) separated by a groove from a less crystalline outer layer (O). Bar = 1 mm. d) Detail of the crystals of the central crystalline mass of the astericus showed weakly hexagonal shape (arrow) with small, rounded nodules at their growing tips (open arrow). Bar = 300  $\mu\text{m}$ .

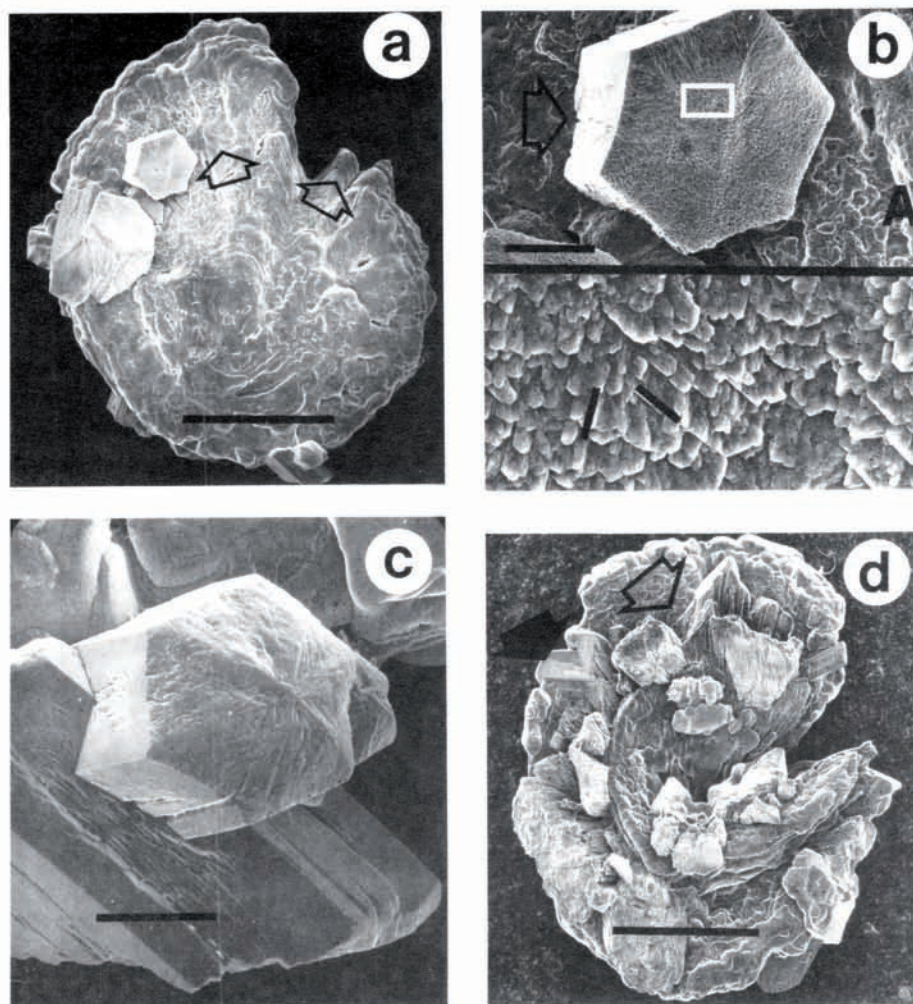
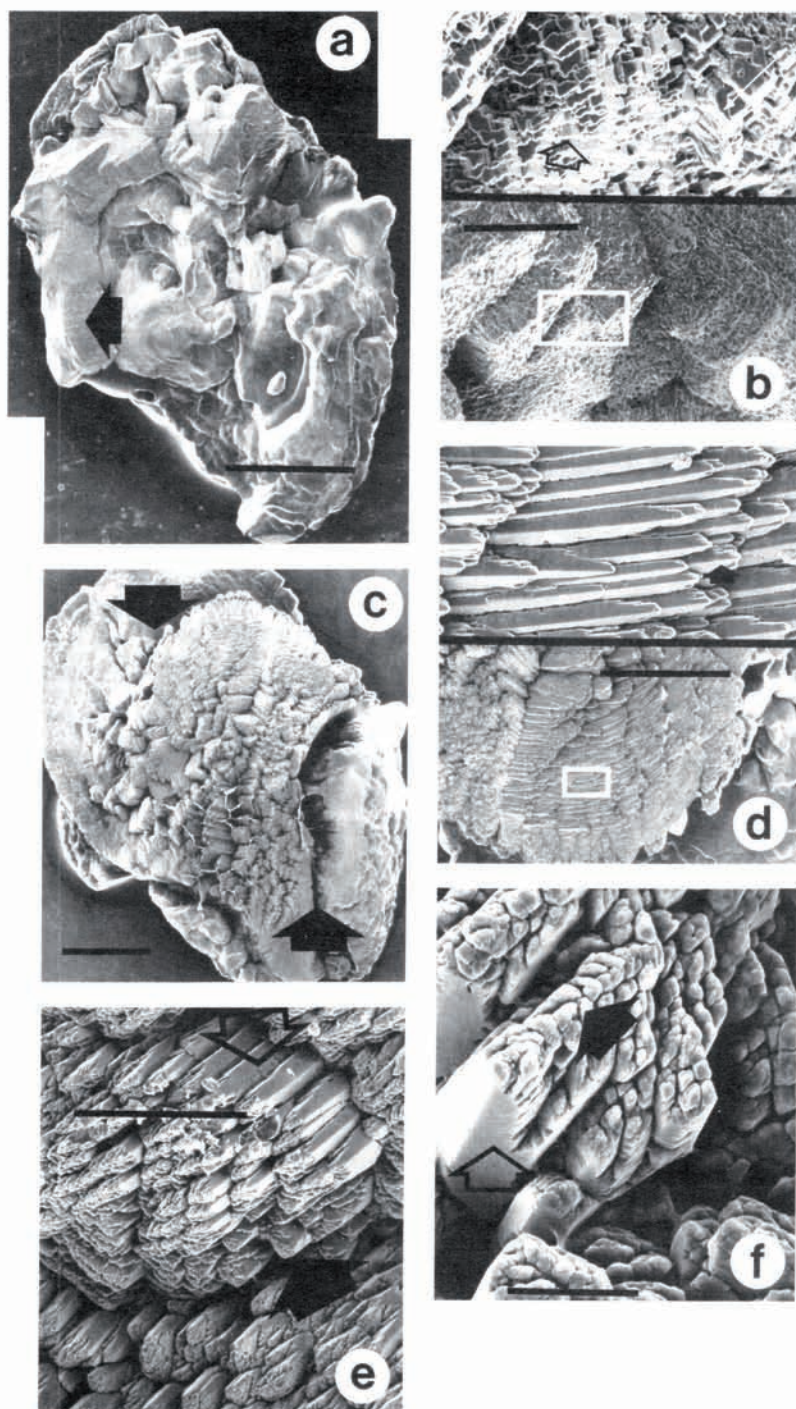


Fig. 6. - The crystalline structure of the anti-sulcal and sulcal surfaces of the second astericus of *Ictalurus punctatus*. a) The anti-sulcal surface of the second astericus grows in concentric bands from a central focus becoming more coarsely crystalline towards the edge, in places forming massive hexagonal twinned crystals. The astericus has a well defined shape with a groove at the point of nerve-entry to the underlying macula, and shows a tendency to form radial prisms (open arrows). Bar = 1 mm. b) Detail of one of the crystals from (d) shows a clear hexagonal shape and a complex lamellar structure in the horizontal plane of the crystal (inset). The hexagonal crystal grows out of a surface that has a lobate, amorphous habit (A) that is completely different to that of the emergent crystal even though they are closely juxtaposed at the crystal surface. Sides of the hexagon are bowed (open arrows) and pitted. Individual lamellae may be seen in the lower magnified section that are organised at about  $64^\circ$  to each other (bars). Bar = 200  $\mu\text{m}$ . c) Detail of another crystal from (d) showed inter-penetrant twinning and a quite different lamellar structure at the apex of the hexagon as well as pitting on the lateral surfaces of the crystals. Bar = 100  $\mu\text{m}$ . d) The sulcal surface of another astericus shows the horseshoe shape typical of the astericus with an inner and outer structure separated by a groove. In this specimen large crystals grew both on the anti-sulcal surface and its edge (arrows). In places, a lobate amorphous surface (open arrows) was closely juxtaposed to large crystals. Bar = 1 mm.



the central horseshoe were oriented vertically to the macula, and the crystals within and surrounding the horseshoe were oriented parallel to the macula. Detail of the central crystalline mass (Fig. 5d) showed narrow monoclinical crystals about 4.5  $\mu\text{m}$  in diameter, ( $n = 11$ ; range 3-7). Some crystals showed weak indications of being half-hexagons with small, round nodules about 2  $\mu\text{m}$  in diameter ( $n = 14$ ; range 1-3). The crystals of the sulcal surface all gave Raman scattering spectra typical of aragonite.

The coarse texture of some of the crystals of the astericus leads to a certain amount of idiosyncratic crystal organisation around the basic shape of the astericus. Although these remarks apply to all of the otoliths of the three catfish species described here, we have included the description of a second astericus from another individual *Ictalurus punctatus* to emphasize two points: that there is in spite of its coarse crystallinity a basic astericus shape for the species, as well as large differences in habit between closely juxtaposed crystals. The anti-sulcal surface of the second astericus was smooth at the focus, with indications of radiating growth (Fig. 6a). The astericus had a distinct groove at the point of entry of the astericus nerve as well as indications of prismatic growth (Fig. 6a). However, growing out of this smooth surface were very large, well formed crystals (Fig. 6a). Detail of one of these crystals showed an hexagonal organisation with lamellar growth on the surface organised around the  $64^\circ$  twinning angle (Fig. 6b). These lamellae grew along the vertical axis and have an average width of about 3.1  $\mu\text{m}$  ( $n = 10$ ; range 2.7-4.2). Another pair of hexagonal crystals showed a different surface at the apex well-developed interpenetrant twinning (Fig. 6c). The sulcal surface of the astericus showed the basic horseshoe shape as well as the coarse crystalline structure typical of the sulcal surface of the astericus of *I. punctatus* in which the crystals grow more parallel to the plane of the macula at the edge of the otolith (Fig. 6d).

#### Lapillus

The lapillus of *I. punctatus* had a coarse anti-sulcal surface consisting of fused and interpenetrant large (up to 1 mm wide) cuboidal crystals (Fig. 7a) arranged more or less concentrically around a poorly developed focus with crystals at the edge larger than at the centre. The crystals of the anti-sulcal surface of the lapillus gave Raman scattering spectra typical of aragonite. Detail of the crystal surface showed steps, kinks and single growth units of the crystal lamellar structure of the large cuboidal crystals (Fig. 7b). The lamellar structure of one crystal was in the form of stacked half-hexagons (Fig. 7b), while other crystals showed co-planarity of growth stacks (Fig. 7b).

The sulcal side of the lapillus was composed of fused and interpenetrant crystals arranged in a rosette-like formation (Fig. 7c). The crystals of the sulcal surface gave Raman scattering spectra typical of aragonite. Detail of the sulcal surface showed long, thin crystals arranged in both the horizontal (Fig. 7d) and vertical planes (Fig. 7e). The long crystals (about 12.5 mm in diameter) showed traces of hexagonal (Fig. 7e) and half-

---

Fig. 7. - Crystalline structure of the anti-sulcal and sulcal surfaces of the lapillus of *Ictalurus punctatus*. a) The anti-sulcal surface of the lapillus shows more-or-less concentric growth from a poorly defined central focus leading to a more coarsely crystalline structure with cuboidal crystals (arrows). Bar = 1 mm. b) Detail of the surface of the cuboidal crystals of (a) shows them to be composed of many small segments inset of lamellae in the form of stacked half-hexagons (arrow), and contiguous crystals showed co-planarity of growth stacks (open arrows). Bar = 200  $\mu\text{m}$ . c) The sulcal surface of the lapillus shows a rosette-like mass of crystals growing from a central focus separated by grooves (arrow) from amorphous crystals at the edges of the otolith. Bar = 1 mm. d) Detail of part of the sulcal surface of (c) shows long crystals growing in the horizontal plane of the otolith with indications of half-hexagonal structure (arrow). Bar = 750  $\mu\text{m}$ . e) Detail of part of the sulcal surface of (c) above shows monoclinical crystals growing in the vertical plane of the otolith. Half-hexagonal structures (arrow) and lamellae (open arrow) are evident. Bar = 100  $\mu\text{m}$ . f) At higher magnification the hexagonal crystals show smooth vertical sides (open arrow) and small growth units (arrow) at the apices of the crystals. Bar = 7.5  $\mu\text{m}$ .

hexagonal (Fig. 7d) structures. Traces of vertical lamellae appeared in some of the long crystals and had an average width of  $1.4\text{ }\mu\text{m}$  ( $n = 11$ ; range  $0.8\text{--}1.7$ ). Detail of crystals (Fig. 7f) showed the basic hexagonal crystal structure with smooth lateral sides and small average  $0.6\text{ }\mu\text{m}$  ( $n = 17$ ; range  $0.3\text{--}0.7$ ) rounded growth units at the apices horizontal plane of the hexagonal crystals.

#### The walking catfish, *Clarias fuscus*

The arrangement of inner ear and location of the otoliths of *Clarias fuscus* are shown in Chardon (1968). The orientation of the otoliths are similar to that of *Ictalurus punctatus* with the lapillus about  $90^\circ$  out of phase with astericus and sagitta.

Fifteen specimens of *Clarias fuscus* were dissected. Although there was some individual variation in the size of the single crystals observed growing in the otolith, the otoliths of *Clarias fuscus* showed a consistent pattern of similar shapes and sizes among individual fishes.

#### Sagitta

The sagitta of *C. fuscus* had a coarsely crystalline anti-sulcal surface (Fig. 8a) composed of large cuboidal blocks of crystals arranged more or less concentrically from a central focus (Fig. 8a). Crystals blocks were smaller than those observed on the sagitta of *I. punctatus* being of the order of  $100\text{ }\mu\text{m}$  in width. The sulcal surface had a double-groove structure similar to that of *I. punctatus* (Fig. 8b) except that the dorsal flute had a more dorsal rotation. The inferior flute of the sagitta of *C. fuscus* was thicker than that of *I. punctatus* but was composed of arrays of crystals with triangular tips growing vertical to the plane of the macula and varying in thickness from about  $5\text{ }\mu\text{m}$  ( $n = 11$ ; range  $3\text{--}9\text{ }\mu\text{m}$ ) in the centre of the flute, to about  $21\text{ }\mu\text{m}$  ( $n = 6$ ; range  $16\text{--}25\text{ }\mu\text{m}$ ) at the sulcal edge

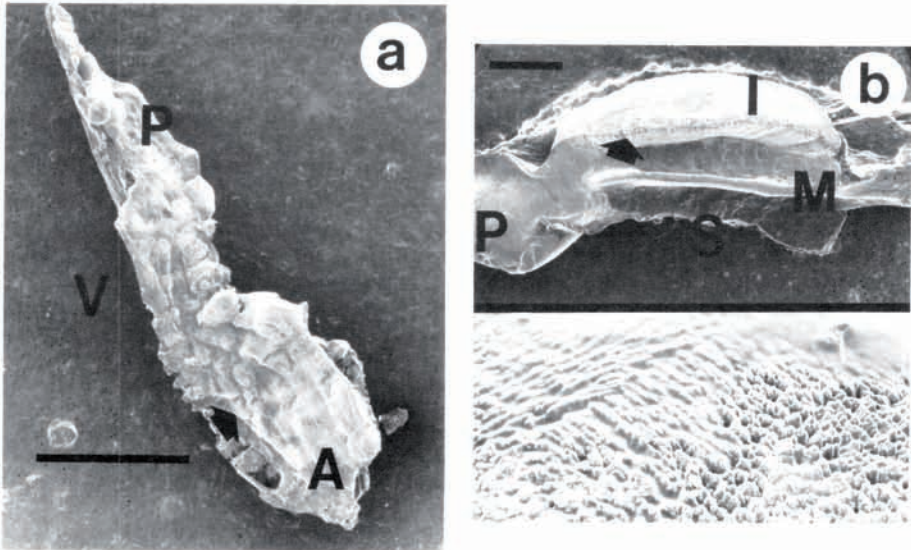


Fig. 8. - Cystalline structure of the anti-sulcal and sulcal surfaces of the sagitta of *Clarias fuscus*. a) The anti-sulcal surface of the sagitta grows more-or-less concentrically from a focus (arrow) located at the anterior (A) end of the otolith, but displaced towards the ventral (V) side of the otolith. The otolith is coarsely crystalline in the posterior segment (P). Bar =  $500\text{ }\mu\text{m}$ . b) The sulcal surface of the sagitta is flattened at the posterior end (P) but has only a partially fluted organisation consisting of an inferior flute (I) along the ventral edge (V), a medial flute (M) and a superior flute (S) that has become a simple lateral projection of the dorsal edge. The inferior flute has a regular crystal structure (inset) composed of wider crystals at the sulcal edge (arrow in upper frame). Bar =  $300\text{ }\mu\text{m}$ .

of the flute (Fig. 8b). Sulcal and anti-sulcal surfaces had Raman scattering spectra typical of aragonite. The sagitta of *C. fuscus* was somewhat thicker for its length, but was in other respects similar to that of *I. punctatus* but without such markedly parallel flutes.

#### Asteriscus

The anti-sulcal surface of the asteriscus of *C. fuscus* was smooth (Fig. 9a) and gave a Raman scattering spectra typical of aragonite. The anti-sulcal surface of the asteriscus of *C. fuscus* typically did not show the large crystals found in the asteriscus of *I. punctatus* and appeared to grow concentrically around a more-or-less central focus (Fig. 9a). The sulcal surface of the asteriscus of *C. fuscus* was roughly horseshoe shaped with a central groove surrounded on three sides by smoothly lobate crystalline material (Fig. 9b). The central crystalline mass gave a Raman scattering spectra typical of aragonite.

The central crystalline mass of the sulcal surface of the asteriscus of *C. fuscus* consisted of long, narrow prisms (about 16:1) with an average diameter of about 75  $\mu\text{m}$  at the growing end (Fig. 9b). Within the central crystalline mass were a number of larger, smooth-surfaced crystals (Fig. 9b). The external part of the otolith consisted of a smooth, lobate surface with weakly defined concentric layers (Fig. 9b).

#### Lapillus

The anti-sulcal surface of the lapillus of *C. fuscus* was flattened and showed a concentric pattern of deposition around a focus centered at the anterior end (Fig. 10a). The posterior half of the anti-sulcal surface of the lapillus had a striated surface that was composed of many crystals of variable widths and highly pitted surfaces (Fig. 10b). The crystals had an average width of about 2  $\mu\text{m}$  ( $n = 27$ ; range 1.8-2.9). In places the hexagonal basic form of the crystal could be seen (Fig. 10b) showing that this surface was basically composed of thin, flat hexagons laying vertical to the surface of the macula.

The sulcal surface of the lapillus of *C. fuscus* was rounded with a rosette of coarse crystals at the centre of the otolith becoming more coarsely crystalline towards the posterior part of the otolith (Fig. 10c) and gave a Raman scattering spectral typical of

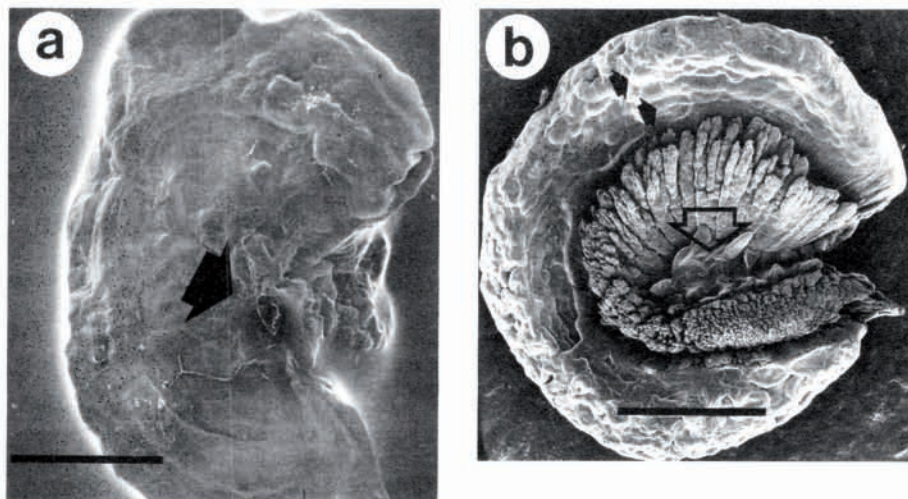


Fig. 9. - Crystalline structure of the anti-sulcal and sulcal surfaces of the asteriscus of *Clarias fuscus*. a) The anti-sulcal surface of the asteriscus grows concentrically from a focus (arrow). Bar = 1 mm. b) The sulcal surface of the asteriscus is horseshoe shaped with a lobate, amorphous outer region separated by a groove from a crystalline inner region that has large smooth crystals (open arrow) growing at the focus and in the central groove of the otolith. Weakly defined concentric layers appear in the outer lobate area (arrows). Bar = 800  $\mu\text{m}$ .

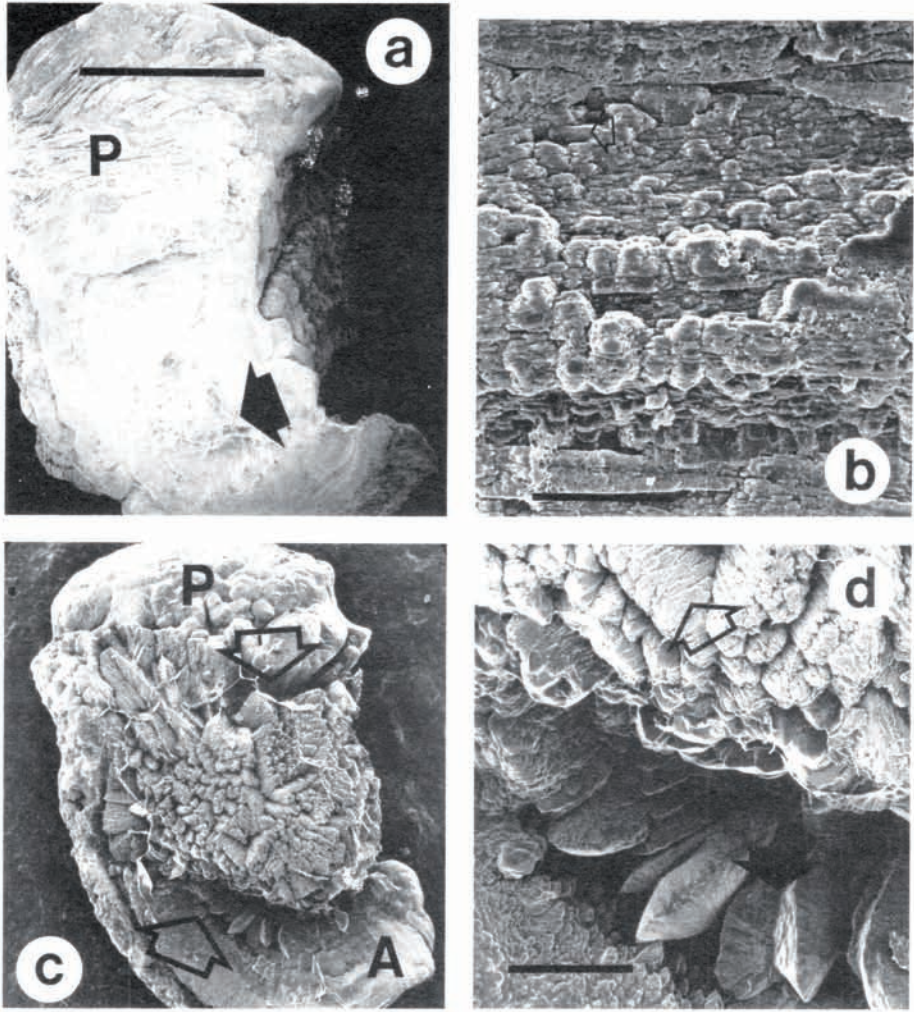


Fig. 10. - Crystalline structure of the anti-sulcal and sulcal surfaces of the lapillus of *Clarias fuscus*. a) The anti-sulcal surface of the lapillus grows more-or-less concentrically from a poorly defined focus (arrow) at the anterior (A) of the otolith. The posterior (P) has a lamellar surface. Bar = 1 mm. b) Detail of the posterior of the anti-sulcal surface of the lapillus shows remnants of a hexagonal crystal structure (arrow) apparently horizontal to the plane of the macula with many small pits in the crystal surface. Bar = 25  $\mu$ m. c) The sulcal surface of the lapillus has a central rosette of crystals with a groove separating (open arrows) much of the sulcal surface from the edge of the otolith. The otolith is smoother at the anterior end (A) than at the posterior end (P). Bar = 1 mm. d) Detail of the central groove in (c) above shows large, hexagonal twinned crystals (arrows) and small hexagonal crystals (open arrows) in the rosette with lateral, smoother faces near the same plane as the macula. Bar = 200  $\mu$ m.

aragonite. Detail of the anterior groove showed large flattened, hexagonal crystals with evidence of twinning at their apices (Fig. 10d). The crystals of the central rosette have a hexagonal appearance with the smoother, lateral surfaces of the hexagon, inclined at a low angle to the plane of the macula (Fig. 10d).

### The loricated catfish, *Hypostomus* sp.

The arrangement of the inner ear and location of the otoliths of *Hypostomus* sp. is shown in Chardon (1968). Eighteen specimens of *Hypostomus* sp. were dissected. Although there was some individual variation in the crystalline structure of the otoliths of the loricated catfish, it was minor compared to the individual variation in the other two species. The otoliths of the loricated catfish (particularly the sagitta) indicated the species-specific shape common to many other teleosts.

#### Sagitta

The anti-sulcal surface of the sagitta of *Hypostomus* sp. showed migration of the most dorsal flute around to the anti-sulcal side (Fig. 11a). The focus of the anti-sulcal surface of the sagitta was marked by a small, round, otoconia-like structure which may be the original primordium of the otolith (Fig. 11a) and was the center of the markedly bowed shape of the sagitta. The upturned edge of the ventral flute showed a tendency to form long thin prismatic crystals (up to 50:1) whose average width along most ventral part of the flute was about 25  $\mu\text{m}$  (Fig. 11a). A series of concentric layers, or steps, cross the anterior end becoming progressively less visible towards the posterior end of the otolith (Fig. 11a). The anti-sulcal surface gave Raman resonance spectra typical of aragonite.

The sulcal surface of the sagitta of *Hypostomus* sp. showed dorsal migration of the medial and superior flutes (Fig. 11b). The inferior flute was greatly thickened with a deep central cavity that showed long, narrow (about 20:1) crystal prisms with an average diameter of about 42  $\mu\text{m}$  at the most ventral edge growing from a central focus (Fig. 11b). The sulcal surface gave Raman spectra typical of aragonite. The sulcal groove between the inferior and median flute was smooth-surfaced developing into an amorphous

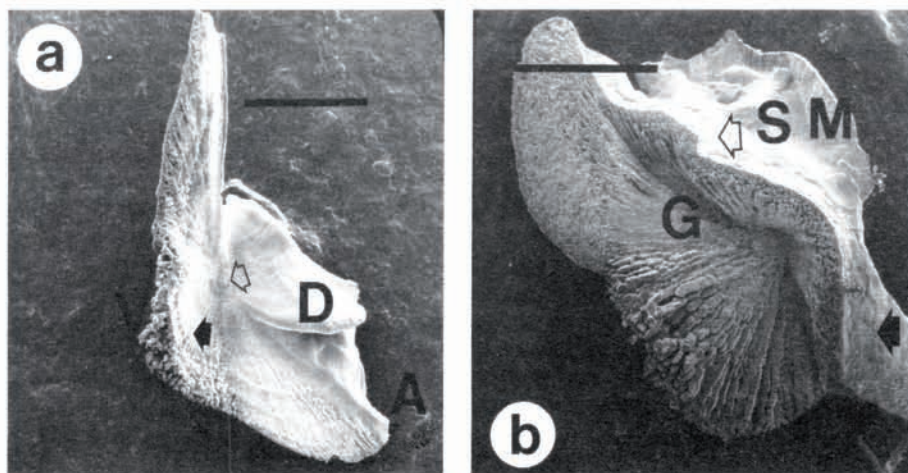


Fig. 11. - Crystalline structure of the anti-sulcal and sulcal surfaces of the sagitta of *Hypostomus* sp. a) The anti-sulcal surface of the sagitta has a concave shape with a slender posterior projection and widened anterior section (A). Parts of the sagitta, particularly the ventral edge (V) are crystalline, but in the form of long prisms (arrow). A clearly defined focus (open arrow) has a spherical structure. Concentric layers or steps cross the anterior section. The superior flute (D) has migrated all the way around to the anti-sulcal surface. Bar = 500  $\mu\text{m}$ . b) The sulcal surface of the sagitta shows a groove (G) within what appears to be the inferior flute. The widened and modified inferior (ventral) flute is separated by a wide, smooth-surfaced groove from the median flute (M) that lies along the dorsal edge of the otolith. The superior flute has moved still further around the otolith and appears as a flattened projection along the dorsal margin of the anti-sulcal surface in (a). The sulcal groove (S) has a smooth surface, that merges with the lobate, amorphous surface of the posterior part of the otolith (arrow) and the ventral wall of the sulcus (open arrow). Bar = 500  $\mu\text{m}$ .

lobate structure along the dorsal edge of the inferior flute and the posterior projection of the otolith (Fig. 11b).

#### *Astericus*

The astericus of *Hypostomus* sp. had a smooth anti-sulcal surface with ridges radiating concentrically from the focus (Fig. 12a) and give Raman spectra typical of aragonite. The anti-sulcal surface of the astericus of *Hypostomus* sp. consistently showed a prismatic structure (Fig. 12a). The surface of the anti-sulcal side of the astericus was composed of very fine-grained rounded crystals (Fig. 12b). These crystals had an average width of about 1.25  $\mu\text{m}$  ( $n = 17$ ; range 0.75-1.6), but some were very small, about 0.75  $\mu\text{m}$  and had the appearance of incipient growth units (Fig. 12b). The central part of the sulcal surface of the astericus was coarsely crystalline with a similar horseshoe-like arrangement of those of *Ictalurus punctatus* and *Clarias fuscus* (Fig. 12c) and large, smooth-surfaced crystals at the centre of the crystalline mass. The crystals of the inner horseshoe were long and narrow (up to 50:1) and had an average width of about 15  $\mu\text{m}$  ( $n = 11$ ; range 11-21  $\mu\text{m}$ ) (Fig. 12c). At the posterior end of the otolith, prisms and lobate structure merged together (Fig. 12c). The anti-sulcal surface had a lobate crystalline habit around the edges of the otolith (Fig. 12a). At higher magnification it is possible to see the transition of crystalline material going from the coarser crystallinity of the central long, narrow prisms to the smoother, more fine-grained crystallinity of the lobate amorphous structure at the otolith edge (Fig. 12d). The amorphous structure of the anti-sulcal surface makes it difficult to detect any clear lamellae. We have assumed, therefore, that the average width of nodules in figure 12d corresponds to the average width of the horizontal (lateral facing) lamellae. The anti-sulcal surface of the astericus had a Raman scattering spectra typical aragonite.

#### *Lapillus*

The lapillus of *Hypostomus* sp. had an irregularly shaped and finely crystalline anti-sulcal surface (Fig. 13a). The sulcal surface of the lapillus of *Hypostomus* sp. was partly formed from stacks of long crystals growing parallel to the horizontal plane of the otolith (Fig. 13b). In the central part of the sulcal surface of the lapillus the stacks of crystals are oriented into a weakly rosette-like structure (Fig. 13b). Most of the sulcal surface was composed of crystals growing with their lateral faces parallel to the surface of the macula, or growing at low angles to the plane of the macula. The average diameter of these crystals was about 13  $\mu\text{m}$  ( $n = 18$ ; range 9-16) and the length to width was about 13:1.

The anti-sulcal surface of the lapillus had a fine-grained structure (Fig. 13a) similar to that of the anti-sulcal surface of the astericus. The anti-sulcal surface showed some indications of concentric growth and prismatic structure (Fig. 13a). The smooth anti-sulcal surface changes abruptly to the coarsely crystalline structure of the sulcal surface (Fig. 13a) visible at the upper edge of the lapillus in figure 13a. Both sulcal and anti-sulcal surfaces of the lapillus gave Raman spectra typical of aragonite.

#### **The sand eel, *Gonorhynchus gonorhynchus***

The anti-sulcal and sulcal surfaces of the sagitta of *Gonorhynchus gonorhynchus* are shown on figures 14a and b respectively.

Three pairs of otoliths were examined and all showed a very similar shape and all had similar arrangements of crystals on the sulcal and anti-sulcal surfaces.

Viewed from the anti-sulcal surface the sand eel sagitta has a well defined nucleus with radiating bands of decreasing width growing towards the dorsal edge of the otolith (Fig. 14a). The bands on the surface are formed by changes in the size of the crystals at the surface (Fig. 14a). The otolith is longer along the anterior-posterior axis than the dorso-ventral axis with the blunt anterior end and a longer pointed posterior end (Fig. 14a).

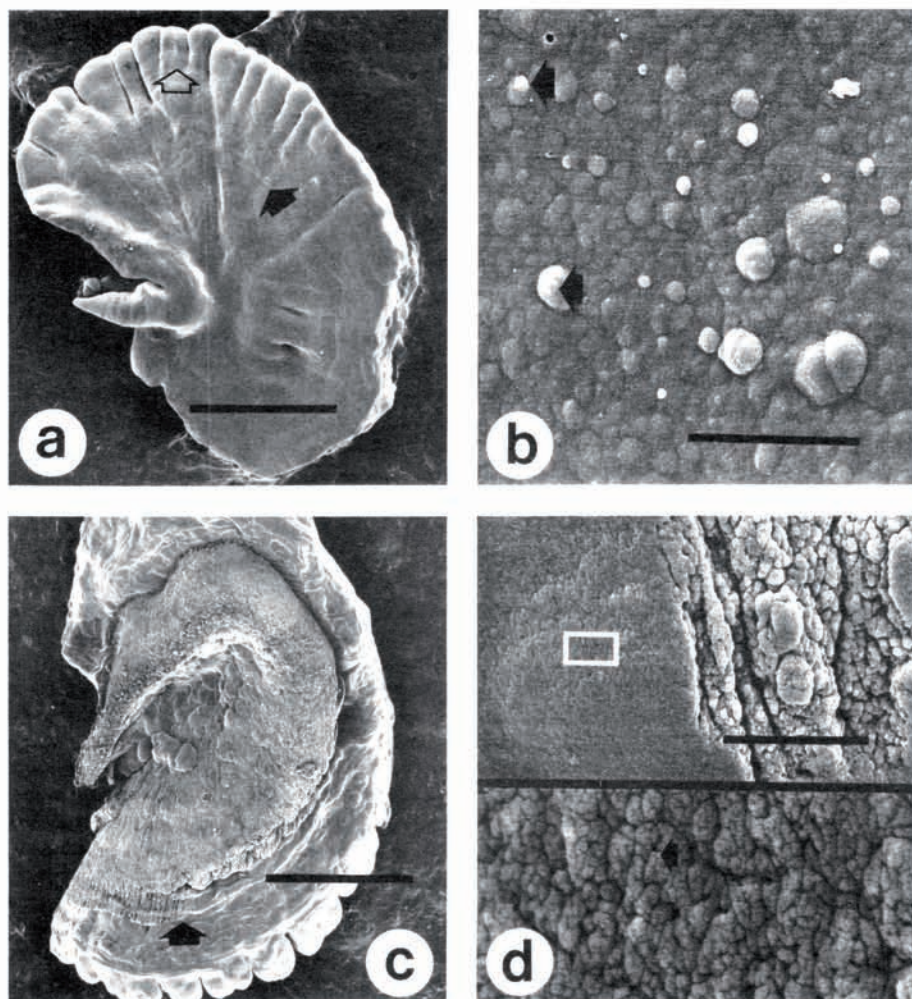


Fig. 12. - Crystalline structure of the anti-sulcal and sulcal surfaces of the astericus of *Hypostomus* sp. a) The anti-sulcal surface of the astericus is flat and smooth with traces of concentric growth (arrow) and indications of developing prisms (open arrow). Bar = 500  $\mu\text{m}$ . b) Detail of the anti-sulcal surface of the astericus from (a) shows a surface composed of smoothed, rounded nodules. Some nodules (arrows) are about 0.75  $\mu\text{m}$  in diameter with the appearance of incipient growth units. Bar = 10  $\mu\text{m}$ . c) The sulcal surface of the astericus has a horseshoe-shaped inner crystalline part separated by a shallow groove from smooth-surfaced lobate, amorphous outer part. Some large crystals grow in the central groove of the inner crystalline part but in places (arrow) smooth and crystalline surfaces merge together. Bar = 500  $\mu\text{m}$ . d) Detail of the sulcal surface of the astericus at the point of merging of the smooth and crystalline surfaces shows both surfaces to have a similar crystal structure, but with different amounts of separation resulting in alternating continuous or discontinuous surfaces. At higher magnifications the surface was composed of small rounded crystals (arrow). Bar = 10  $\mu\text{m}$ .

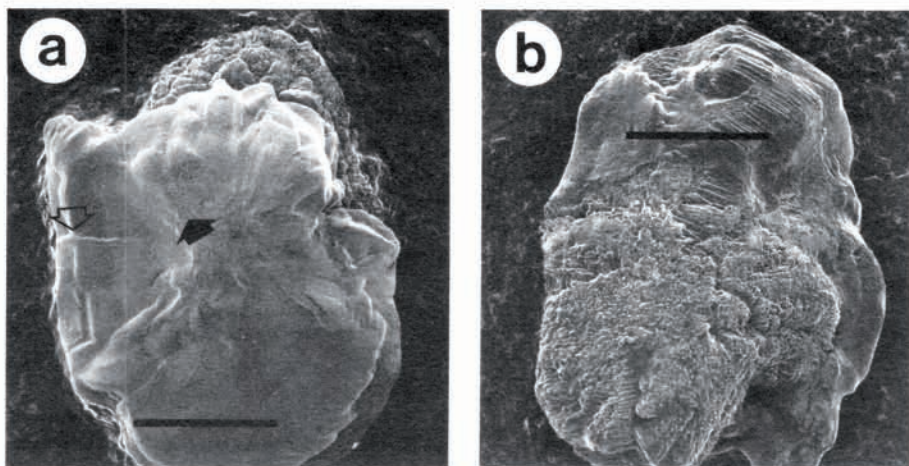


Fig. 13. - Crystalline structure of the anti-sulcal and sulcal surfaces of the lapillus of *Hypostomus* sp. a) The anti-sulcal surface of the lapillus is smoothly crystalline with both radial (arrow) and concentric elements (open arrows). Bar = 500  $\mu\text{m}$ . b) The sulcal surface of the lapillus has a central crystalline region in an otherwise fairly shapeless structure of monoclinical crystals. Bar = 500  $\mu\text{m}$ .

The sulcal surface of the sand eel sagitta showed a number of features that are analogous with those of the catfish sagitta. The sulcus appears to be divided into a deeper, ventral section, and a more shallow dorsal section (Fig. 14b) that gives rise to three structures analogous to the superior, median and inferior flutes of the catfish otoliths.

Detail of the sulcal surface of the sagitta reveals a number of crystal habits similar to those observed in the catfish otoliths. The posterior end of the dorsal ramus (marked in Fig. 14b), showed at higher magnification stacks of long monoclinical aragonitic crystals (Fig. 14c) similar to those at the posterior end of the dorsal ramus in *Hypostomus* sp. (Fig. 11b). Crystals had an average diameter of 1.3  $\mu\text{m}$  ( $n = 19$ ; range 1-1.5) a length of about 200  $\mu\text{m}$  ( $n = 20$ ). The crystals had small growth units on their surfaces with an average diameter of about 10.6  $\mu\text{m}$  ( $n = 18$ ; range 8-12). Crystal habit changed towards the anterior end of the dorsal part of the otolith leading to a layered structure (Fig. 14b). Detail of the layered structure showed a highly laminated surface leading block-like crystalline masses (Fig. 14d) that were composed of arrow lamellae (Fig. 14e). The width of lamellae at the surface of the crystal blocks in figure 14e was very narrow, of the order of 0.05  $\mu\text{m}$ , but lamellae within the crystal blocks (Fig. 14e) were much wider, about 1.6  $\mu\text{m}$  ( $n = 19$ ; range 1.1-1.8). In the context of the crystal structure it is likely that the width of the very narrow surface lamellae are equivalent to the diameters of growth units, and more likely to be those typical of the crystal. Lamellae in both the horizontal and vertical planes have about the same width resulting in the approximately cuboidal shape of the crystal blocks.

The anterior end of the ventral edge of the sulcal side of the sagitta of *G. gonorhynchus* was composed of triangular shaped crystals (Fig. 14f). Many of these triangular crystals were organised around the 64° angle typical of twinned aragonite (Fig. 14f).

Information related to crystal dimensions, including crystal lamellae width and crystal shape is summarized by species and by otolith in table I. The length-to-width ratios of otoliths are shown by species and otoliths in table II.

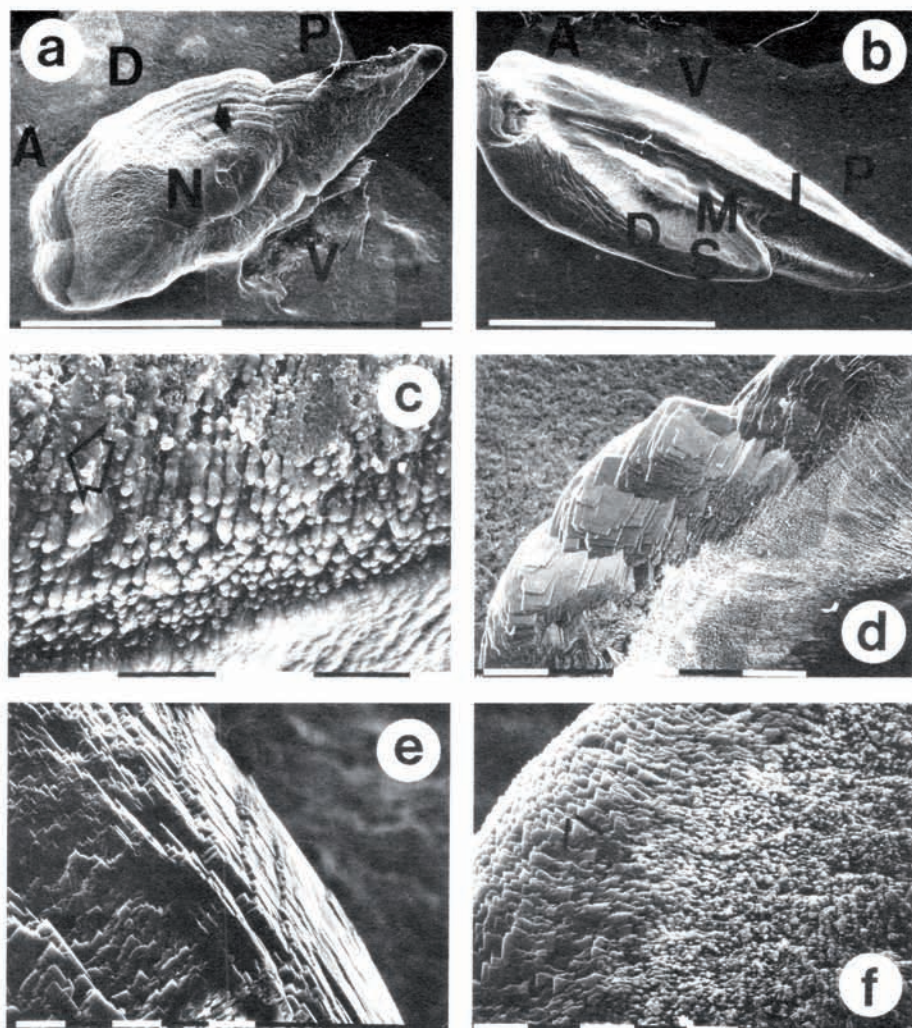


Fig. 14. - The crystalline structure of anti-sulcal and sulcal surfaces of the sagitta of *Gonorhynchus gonorhynchus*. a) The anti-sulcal surface of the sagitta is longer anterior-posterior (A, P) than dorsal-ventral (D, V) with a well-developed apical nucleus (N) and radiating bands (arrows) arising from variations in crystal size. Bar = 1 mm. b) The sulcal surface of the sagitta is divided into deeper ventral (V) and shallower dorsal (D) grooves by structures analogous to the superior, median and inferior flukes (S, M, I with arrows). Crystal structure changes from the posterior dorsal ramus (P) towards the anterior (A) of the sagitta. Bar = 1mm. c) Detail of the posterior end of the dorsal ramus of the sulcal side of the sagitta shows long crystals with small growth units (arrow) on their surfaces. Bar = 10  $\mu$ m. d) The anterior end of the dorsal ramus of the sulcal side of the sagitta shows block-like crystals formed by flat lamella. Bar = 100  $\mu$ m. e) Detail of the crystals at the anterior end of the dorsal ramus of the sulcal side of the sagitta shows the lamellar structure. Bar = 10  $\mu$ m. f) Detail of crystals at the anterior ventral edge of the sulcal side of the sagitta shows an array of triangular crystals organised around the  $64^\circ$  angle of aragonite (intersecting lines). Bar = 10  $\mu$ m.

Table II - Length-to-width ratios of catfish otoliths are shown by species and otolith. Average ratios are shown with the range of values in brackets.

| Otolith   | <i>I. punctatus</i> | <i>C. fuscus</i> | <i>Hypostomus</i> sp. | <i>G. gonorhynchus</i> |
|-----------|---------------------|------------------|-----------------------|------------------------|
| Sagitta   | 3.47 (3.45-3.49)    | 3.83 (3.27-4.39) | 2.26 (2.14-2.38)      | 2.7 (2.55-2.92)        |
| Astericus | 1.24 (1.19-1.30)    | 1.06 (1.06-1.07) | 1.57 (1.44-1.70)      | -                      |
| Lapillus  | 1.38 (1.26-1.50)    | 1.58 (1.55-1.61) | 1.38 (1.36-1.39)      | -                      |

## DISCUSSION

Our observations of the structure of the otoliths of *Ictalurus punctatus*, *Clarias fuscus*, *Hypostomus* sp., and *Gonorhynchus gonorhynchus* raise mineralogical, physiological and systematic issues.

### Mineralogy

All of the otoliths described here were aragonitic. Occasionally otoliths of other teleost species have large surface crystalline structures formed from morphs of calcium carbonate other than aragonite, including calcite and vaterite (Campana, 1983; Gauldie, 1986; Strong *et al.*, 1986; Gauldie, 1990). Formations of aragonite crystals that are unusually large for teleost otoliths occur in otoliths of Oreosomatid fishes (Davies *et al.*, 1989), but no teleost otoliths have been reported to have the massive cuboidal aragonite crystals of the size observed on the sagitta, astericus, and lapillus of some of the otoliths described here.

Variation in crystal shape, or more properly variation in crystal habit, occurs in all biogenic calcium carbonates (Carriker *et al.*, 1980) but not usually with such a steep gradient in the size of juxtaposed crystals. The sagitta and astericus of all three catfish species showed very large single crystals growing next to an amorphous surface composed of minute crystals. Some types of crystals, such as the long crystals of the inferior flute of the sagitta and the triangular chamfered edge crystals of the inferior flute persisted through all three catfish species as well as *Gonorhynchus gonorhynchus*. Crystal size decreased progressively from *Ictalurus punctatus*, through *Clarias fuscus*, to *Hypostomus* sp., but crystals in *Gonorhynchus gonorhynchus* were, on average, much smaller than in catfishes.

The cuboidal crystals observed in catfish otoliths were dissimilar from the cuboidal calcite crystals that occurred in the otoconial mass homologous to the teleost otolith in some shark species (Mulligan and Gauldie, 1989). The cuboidal crystal in sharks was tilted into the "iceland spar" shape and had a completely different lamellar structure in which the lamellae were oriented at a different angle (Mulligan and Gauldie, 1989) to those observed in the cuboidal catfish otolith. Aragonite sometimes occurs in a tablet formation that ranges from a rectangular to hexagonal cross-section (Wise, 1970; Mutvei, 1980). The cuboidal crystals observed here may be layers of massive rectangular aragonite tablets. Following Mutvei's (1980) description of nascent aragonite tablets in the shell of *Mytilus edulis*, one would expect the crystal lamellae of an aragonite tablet to be oriented at right angles to each other, which, in some of the cuboidal crystals described here (e.g. Fig. 3b), they appear to be.

Large, hexagonal single crystals grew on the anti-sulcal surface of the astericus of *Ictalurus punctatus* and *Clarias fuscus*. The bowing of some of the lateral sides of these hexagonal crystals (e.g. Fig. 3f) indicate that these crystals may be pseudo-mimetic aragonite twin crystals (McKie and McKie, 1986). The organisation of the lamellae growing at the apex of the large, hexagonal crystals also suggests twinning because the lamellae intersect at the approximately 64° angle the twinning angle (63°48') observed in

other otolith aragonites (Gauldie and Nelson, 1988). The hexagonal crystals observed in some otoliths express the more commonly observed flattened hexagonal crystals of aragonite in mollusc shells and otoliths. The flattened hexagon habit can also be seen in the stacked half-hexagons observed at the apices of some cuboidal crystals (Fig. 3c). An unusual variation on the hexagonal crystal was observed in crystals lying within the sulcal groove of the sagitta of *I. punctatus* (Fig. 4e). These crystals were characterised by almost no growth of the lateral faces of the crystal and a smooth apical surface with minute superficial crystals. The sulcal groove of the sagitta of all three species had the same smooth surface with minute crystals. This essentially amorphous kind of surface showed a lobate structure in other parts of the sagitta, and at the edges of the astericus.

Biogenic calcium carbonate crystals show a wide variety of habits within any one morph (Carriker *et al.*, 1980; Wilbur and Saleuddin, 1983). Although the resulting morphological complexity can look chaotic, of all the underlying crystals of aragonite must take up one of limited number of stereochemical orientations of calcium and carbonate ions in order to form aragonite at all. This kind of stereochemical constraint results in a standard relationship between faces of crystals. Aragonite has basically an orthorhombic organisation that should lead to a rectangular (or parallelogram) cross section of laths or plates. However, the arrangement of calcium and carbonate that allows the tighter molecular packing of aragonite, also results in a pseudo hexagonal internal structure which readily translates into crystals with the external appearance of hexagons as a result of twinning. Our examination suggests that in the catfish otoliths the commonly occurring crystal habit is the hexagonal form with a broad face and narrower faces at the apices. This organisation would result in the half-hexagon stacking at the unstable, faster growing faces of the cuboidal crystals as well as large and small flattened hexagons. Studies of artificial calcium maleate crystals grown in the presence of glycoproteins extracted from mollusc shells have shown stable (and therefore slower) growth at the lateral faces, with unstable growth faces presumably resulting from higher affinities for the lateral faces by the protein (Addadi and Weiner, 1985).

However, the twinning necessary for maintaining the less-stable hexagonal form implies a directly opposite effect, the simultaneous growth in two directions of one of the internal faces of the crystal. If one accepts the argument that the shape of biogenic calcium carbonate crystals is generated by matrix proteins (Lowenstam and Weiner, 1989; Simkiss and Wilbur, 1989; Mann *et al.*, 1989), then there may be at least two stereochemically active proteins at work in the crystals of the catfish otolith: one protein that accelerates growth at the twinning face, and another that inhibits growth at the lateral face that leads to elongate crystals. The observed orientation of crystals could therefore be regarded as a series of tradeoffs between the stereo-chemical effects of these two proteins on the permitted direction of growth, and the rate limiting physical chemical effects that control the availability of calcium and carbonate ions that effect the permitted rate of growth (Addadi and Weiner, 1985; Weissbuch *et al.*, 1991).

The extremes of this process would range from no growth at the lateral faces, to twinning at all faces. The large hexagonal crystals observed in the sulcus in figure 4e showed very restricted lateral growth with almost no growth of the lateral faces developed on the crystal. The other extreme can be seen in the large hexagonal and cuboidal crystals of the anti-sulcal surfaces in which either extensive twinning of the lateral faces or extensive growth of the lateral faces of the crystals occur but not both. An intermediate form can be seen in the individual crystal of the figure 5b in which the twinning effect is strong enough to ensure co-planarity in the homologous axes of the lateral faces, but the inhibition of the lateral face still occurs leading to a rather skeletal-looking crystal with the appearance of having been eroded.

In the four species described here some of the same crystal shapes persist not only through the otoliths of the three catfishes but also in the otolith of the sand eel *Gonorhynchus gonorhynchus*. Even though otolith shape changes between *G. gonorhynchus* and the catfishes, there is still a similarity between *G. gonorhynchus* and

the catfishes at the more fundamental mineralogical level. If the mineralogy of the otolith is controlled by different organic matrices as the mineralogical arguments imply, then the same matrix material would have to be expressed in all four of the species described here. However, genetic regulation of the variation in matrix production would then provide a parsimonious mechanism for the allometric reorganization of the basic crystal fields that lead to the change in otolith shape from *G. gonorhynchus* to *Hypostomus*.

### Physiology

The four fish species used in this study are drawn from four families Gonorhynchidae, Ictaluridae, Bagridae and Loricariidae, that are regarded as roughly representative of a range from anatomically primitive, to the anatomically more sophisticated (Jenkins, 1977; Fink and Fink, 1987). The progress from coarsely crystalline and relatively simply organised sagitta and astericus otoliths of *Ictalurus punctatus*, through those of *Clarias fuscus*, to the more finely crystalline and more complex organization of the sagitta and astericus of *Hypostomus* sp., that apparently reflects evolution of the otolith within the catfishes. The mineralogical similarities of *Gonorhynchus* otoliths of those of the catfishes reinforces the status of the sand eel as a primitive ostariophysine fish. If we accept this phylogenetic scenario, we are then left with the questions of what would drive such an increase in apparent sophistication of otolith structure within the catfishes, yet at the same time account for the apparent decrease in sophistication that took place between *G. gonorhynchus* and *I. punctatus*? The answer to this question must surely lie in some progressive changes in their physiology that follows the form of otoliths from *G. gonorhynchus*, through *I. punctatus* and *C. fuscus* to *Hypostomus* sp. There are two readily observable sources of information in the otolith that relate from physiological function, otolith size and otolith shape; both of which are related to the size and organization of the crystals that form the otolith.

Crystals size has been examined in relatively few otoliths (Dunkelberger *et al.*, 1980; Gauldie and Nelson 1990; Gauldie, 1991). Crystal size decreases between *I. punctatus*, *C. fuscus* and *Hypostomus* sp. Crystal widths (from Table I) change from average width of about 369  $\mu\text{m}$  (range 4.5-1000  $\mu\text{m}$ ) in *I. punctatus* through 41  $\mu\text{m}$  (range 2-100  $\mu\text{m}$ ) in *C. fuscus* to 19  $\mu\text{m}$  (range 1.25 to 42  $\mu\text{m}$ ) in *Hypostomus* sp. The length-to-width ratios also change from an average of 8.5:1, through 16:1 to 33:1 for the three catfish species. Crystal size in *G. gonorhynchus* does not follow this trend, being smaller than in the three catfish species. Widths of crystal lamellae were more difficult to measure, but varied from 4.3 and 2.7  $\mu\text{m}$  in *I. punctatus*, down to about 0.58 mm in *Hypostomus* sp. Lamellae in *G. gonorhynchus* otoliths were of the same order of those in *I. punctatus*, reflecting the commonality of the large cuboidal type of crystal in the otoliths of both species. The observed pattern among the catfish otoliths was one of decreasing crystal width accompanied by an increase in crystal length, but the longest crystals were observed in *G. gonorhynchus*. Crystal size is related to crystal growth rate. Therefore given two otoliths of the same dimension, smaller crystal size means faster growth rate of the otolith and consequently younger age.

It is evident from table II that the shape of the lapillus has been conserved in the three catfish species. The astericus of *Hypostomus* sp. has become more elongate, but the shape of the astericus of *I. punctatus* is similar to that of *C. fuscus*. The shapes of the sagittae of *I. punctatus* and *C. fuscus* remain similar, but the shape of the sagitta of *Hypostomus* sp. is different from the other two species. The shape of the sagitta of *G. gonorhynchus* is the least specialised with weak ridges on the sides of the double sulcus rather than a recognisably fluted structure.

Changes in the dimensions of the otolith, changes in crystal size, and (although less well supported) changes in the width of crystal lamellae, all point to a progressive change in the basic organisation of the crystal of the otolith that accompanies the changes in gross anatomy of the otoliths from *G. gonorhynchus*, *I. punctatus*, through *C. fuscus* to *Hypostomus* sp.

One approach to the problem of what may drive this progressive change was indirectly suggested by Blaxter *et al.* (1981) in their study of the mechanics of the gas bladder connection to the inner ear of clupeid fishes. They pointed out that there were two possible components in the mechanics of sound reception. One component was the initial effect of an incoming wave front which would be immediately detected as a noise, i.e. a rapid acceleration in the relative displacement of the mass/macula coupling. The other component was the cycle of displacements of the mass/macula coupling that follows the cycle of the frequency dependant message contained in the incoming sound waves. To detect the frequency dependent message of an incoming sound signal the whole cycle of the message would have to pass through the mass/macula coupling. Blaxter *et al.* (1981) pointed out the biological advantages of rapid noise reception associated with the wave front, coupled with message received from the whole sound cycle. From a mechanical point of view, noise detection has the added advantage of occurring both by movement of mass with respect to macula, or the reverse, macula movement with respect to mass.

All mass/macula couplings (including those of gravity and angular momentum detectors) must physically respond to displacement by pressure waves, as well as by tilt and displacement by angular momentum. Therefore all otoliths have the potential to hear both the noise and message components. However, the progressive rotation of flutes observed in sagitta from *I. punctatus* to *Hypostomus* sp. may imply an increasing sensitivity to the frequency component of the sound. This follows from the increase in sensitivity to displacement of the otolith as its asymmetry increases (Schuif, 1981). Under these circumstances increasing the mass of the lapillus would make the mass/macula coupling of the lapillus progressively more insensitive to a frequency message that depends on the rotation of the otolith, but would maintain both the gravitational (tilt) function, and noise reception that can be achieved by moving the macula, not the otolith. This would account for the relatively large size of the lapillus and the large macula area associated with the lapillus. It has been argued from the mechanics of otolith rotation (Gauldie, 1988) that the large area of the macula relative to the otolith that is typical of the lapillus indicates a sensitivity to tilt, rather than the frequency transducer role typical of the sagitta (Fay, 1984). Indirect support for this argument comes from the study of the physiology of the inner ear of the catfish *Arius felis* by Popper and Tavalga (1981). The lapillus of *A. felis* is very large and the macula has rotated to the upper surface of the lapillus and has the form of an equatorial band. *Arius felis* produces short intense pulses (5-10 ms) of sound at about 100Hz that Popper and Tavalga (1981) suggested may be used as part of a simple echolocation mechanism. Such short, intense pulses can be regarded as noise in terms of our discussion. Although Popper and Tavalga (1981) made no claims for specific noise reception by the lapillus, there are parallels between both arguments.

The inner ear of another ostariophysine fish, the gold fish, was examined for differences in the role of otoliths by Furukawa and Ishii (1967). They showed that the sagitta of the goldfish responds to a wide range of sounds, while the astericus responds only to sounds of sufficient intensity to cause the head of the fish to vibrate. They did not investigate the lapillus. Although not a catfish, the sagitta of the goldfish has a fluted structure, and the astericus is very similar in shape to that of the catfishes (Furukawa and Ishii, 1967).

### Systematics

So far in our discussion we have argued that the mineralogy of the otolith have become progressively more complex, and that a reasonable physiological case can be proposed to account for that increase in complexity. Can this information be applied to catfish systematics? Studies of the evolution of the inner ear of the mole rat, *Spalax*, have shown a continuous (and continuing) evolution of inner ear structure and function among mole rat species, and between phenotypes within species (Nevo, 1991). We propose that

our small sample can be used to establish an hypothesis of inner ear evolution in catfishes.

The catfishes have been described by Fink and Fink (1982) as a sister-group within the Ostariophysine fishes. However, the most primitive Ostariophysine fishes, the Gonorhynchids, have simple otoliths compared to the catfish. The coarsely crystalline structure observed in catfish otoliths appears to have developed within the catfishes, and is not a primitive character of ostariophysine fishes. Flutes along the sulcal groove also occur in non-ostariophysine fishes, e.g. *Antimora rostrata* (Gauldie *et al.*, 1991) as well as in other groups within the ostariophysine fishes, e.g., the Cypriniformes (Furukawa and Ishii, 1967; Nolf, 1985), so flutes, too, are not a primitive ostariophysine character.

If the crystalline changes that have occurred in the sequence of otoliths from *G. gonorhynchus* through *I. punctatus* to *Hypostomus* sp. have been mediated by different matrix proteins (or other organic molecules, e.g. polysaccharides that may be associated with the matrix) then at least part of the genetic basis of evolution of otolith shape in the catfishes must lie in the genes coding for the organic matrix. Amino acid variation in matrix proteins of calcium carbonates is known to occur at higher taxonomic levels than the species (Degens *et al.*, 1969; Ross *et al.*, 1981; Meenakshi *et al.*, 1985) and can therefore be expected to also occur at the species level. However, the basic mineralogical structures that persist through the otoliths described here occur simultaneously in the same otolith. If there is a genetic basis to such structures, then it is in the form of different genes being expressed simultaneously. This is not a genetic polymorphism in the sense of a succession of different genes at the same locus, but rather a genetic ensemble of genes expressed simultaneously. In addition, changes in otolith shape reflect the relative amounts of the different mineral structures as well as changes in their relative growth rates. Modulation of the amount and growth rate of the different mineral structures must be controlled by the cells of the macula. There is already evidence of a neurosecretory role for the macula cells in *Hoplostethus atlanticus* (Gauldie and Nelson, 1988). The uptake of matrix proteins from the macula into the fish otolith has been observed by Zhang (1992). Development of neurosecretory control over the growth fields of the catfish otolith would imply that the same structural otolith genes are shared by the most sophisticated and primitive ostariophysine fishes, and that it has only been necessary to regulate the expression of those genes to develop the species-specific shapes of catfish otoliths.

Their approach implies a constant set of structural genes that produce the minerals that characterize the whole order of catfish otoliths, and regulatory genes that modulate the crystal growth rates responsible for the allometric shifts in otolith morphology that characterize particular species within the order. This hypothesis implies a potentially continuous range of otolith size and shape that is effectively sub-sampled by the evolutionary process and thereby appears to our view as a series of discrete, discontinuous species-specific otoliths.

**Acknowledgements.** - We thank Dennis Shimno and Mike Yamamoto of the Hawaii State Forestry Department for assistance in the supply of catfish. This project was supported by a Seed Money Grant from the University Research Council, University of Hawaii. SOEST contribution no. 3294.

## REFERENCES

- ADDADI L. & S. WEINER, 1985. - Interactions between acidic proteins and crystals: stereochemical requirements in biomineralization. *Proc. natl. Acad. Sci. U.S.A.*, 82: 4110-4114.
- APPELGATE J. & L.L. SMITH, 1951. - The determination of age and rate of growth from vertebrae of the channel catfish, *Ictalurus lacustris punctatus*. *Trans. Am. Fish. Soc.*, 80: 119-139.

- BISCHOFF W.D., SHARMA S.K. & F.T. MACKENZIE, 1985. - Carbonate ion disorder in synthetic and biogenic magnesian calcites: a Raman spectral study. *Am. Miner.*, 70: 581-589.
- BLAXTER J.H.S., DENTON E.J. & J.A.B. GRAY, 1981. - Acousticolateralis system in clupeid fishes. pp. 39-60. In: Hearing and sound communication in fishes (Tavolga W.N., Popper A.N. & R.R. Fay, eds), Springer-Verlag, Berlin.
- BLOSS F.D., 1971. - Crystallography and Crystal Chemistry. 545 pp. Holt, Rinehart and Winston, New York.
- CAMPANA S.E., 1983. - Calcium deposition and otolith check formation during periods of stress in coho salmon, *Oncorhynchus kisutch*. *Comp. Biochem. Physiol.*, 75: 215-220.
- CARRIKER M.R., PALMER R.E. & R.S. PREZANT, 1980. - Functional ultramorphology of the dissoconch valves of the oyster *Crassostrea virginica*. *Proc. natl. Shellfish. Assoc.*, 70: 139-183.
- CHARDON M., 1968. - Anatomie comparée de l'appareil de Weber et des structures connexes chez les Siluriformes. *Ann. Mus. Roy. Afr. cent.*, Tervuren, Belgium. Sciences Zoologiques, 169, 277 pp.
- DALE T., 1976. - The labyrinthine mechanoreceptor organs of the cod *Gadus morhua* L. (Teleostei: Gadidae). *Norw. J. Zool.*, 24, 85-125.
- DAVIES N.M., GAULDIE R.W., CRANE S.A. & R.K. THOMPSON, 1989. - The crystalline structure of the otoliths of the oreos *Pseudocyttus maculatus* and *P. allocyttus* sp. *Fish. Bull.* 85: 103-115.
- DEAN J.M., WILSON C.A., HAAKE P.W. & D.W. BECKMAN, 1983. - Microstructural features of teleost otoliths. pp. 353-559. In: Biomineralization and Biological Metal Accumulation. Reidel Publishing Co.
- DEGENS E.T., DEUSER W.G. & R.L. HAEDRICH, 1969. - Molecular structure and composition of fish otoliths. *Mar. Biol.*, 2: 105-113.
- DUNKELBERGER D.-G., DEAN J.M. & N. WATABE, 1980. - The ultrastructure of the otolithic membrane and otolith in the juvenile mummichog, *Fundulus heteroclitus*. *J. Morphol.* 163: 367-377.
- FAY R.R., 1984. - The goldfish ear codes the axes of acoustic particle motion in three dimensions. *Science*, 225: 951-953.
- FINK S.V. & W.L. FINK, 1987. - Interrelationships of the ostariophysine fishes (Teleostei). *Zool. J. Linn. Soc.*, 72: 297-353.
- FURUKAWA T. & Y. ISHII, 1967. - Neurophysiological studies on hearing in goldfish. *J. Neurophys.*, 30: 1377-1403.
- GAEMERS P.A.M., 1984. - Taxonomic position of the Cichlidae (Pisces: Perciformes) as demonstrated by the morphology of their otoliths. *Neth. J. Zool.*, 34: 566-595.
- GAULDIE R.W., 1986. - Vaterite otoliths from chinook salmon (*Oncorhynchus tshawytscha*). *N.Z. J. Mar. Freshw. Res.*, 20: 209-217.
- GAULDIE R.W., 1988. - Function form and time-keeping properties of otoliths. *Comp. Biochem. Physiol.*, 91: 395-402.
- GAULDIE R.W., 1990. - Vaterite otoliths from the Opah, *Lampris immaculatus*, and two species of sunfish, *Mola mola* and *M. ramsayi*. *Acta Zool., Stockh.*, 71: 193-199.
- GAULDIE R.W., 1991. - The morphology and periodic structures of the otolith of the chinook salmon (*Oncorhynchus tshawytscha*), and temperature dependent variation in otolith microscopic growth increment width. *Acta Zool., Stockh.*, 72: 159-179.
- GAULDIE R.W. & D.G.A. NELSON, 1988. - Aragonite twinning and neuroprotein secretion are the cause of daily growth rings in fish otoliths. *Comp. Biochem. Physiol.*, 90: 501-509.
- GAULDIE R.W. & D.G.A. NELSON, 1990. - Interactions between crystal ultrastructure and microincrement layers in fish otoliths. *Comp. Biochem. Physiol.*, 97: 449-459.
- GAULDIE R.W., COOTE G., MULLIGAN K.P., WEST I.F. & N. MERRETT, 1991. - Otoliths of deep water fishes: structure, chemistry and chemically coded life histories. *Comp. Biochem. Physiol.*, 100: 1-32.
- JENKINS D.G., 1977. - A light microscopic study of the saccule and lagena in certain catfishes. *Am. J. Anat.*, 150: 605-630.
- JENKINS D.G., 1979. - A transmission and scanning electron microscopic study of the saccule in five species of catfishes. *Am. J. Anat.*, 154: 81-102.
- LOWENSTAM H.A. & S. WEINER, 1989. - On Biomineralization. 324 pp. Oxford University press, New York and Oxford.
- MANN S., WEBB J. & R.J.P. WILLIAMS, 1989. - Biomineralization: Chemical and Biochemical Perspectives. 541 pp. VCH Verlag, Weinheim.

- McKIE D. & C. McKIE, 1986. - Essentials of Crystallography. Blackwell Scientific Publications. Oxford and London.
- MEENAKSHI V.T., HARE P.E. & K.M. WILBUR, 1985. - Amino acids of the organic matrix of neogastropod shells. *Comp. Biochem. Physiol.*, 40: 1037-1043.
- MULLIGAN K.P. & R.W. GAULDIE, 1989. - The biological significance of the variation in crystalline morphology and habit of otoconia in elasmobranch. *Copeia*, 1989: 857-871.
- MUTVEI H., 1980. - Ultrastructural characteristics of the nacre of some gastropods, pp. 49-65. In: The Mechanisms of Biomineralization in Animals and Plants (Onori M. & N. Watabe, eds). Tokai Press, Tokyo.
- NEVO E., 1991. - Evolutionary theory and processes of active speciation and adaptive radiation in subterranean mole rats, *Spalax ehrenbergi* superspecies, in Israel. *Evol. Biol.*, 25: 1-125.
- NIELSEN A.E. & J. CHRISTOFFERSEN, 1982. - The mechanisms of crystal growth and dissolution, pp. 37-78. In: Biological Mineralization and Demineralization, (Nancollas G.H., ed.). Springer-Verlag Berlin, Heidelberg, New York.
- NOLF D., 1985. - Otolithi piscium, p. 1-145. In: Handbook of Paleichthyology, Vol. 10. (Schultze H.-P., ed.). Gustav Fischer, Stuttgart.
- PANELLA G., 1980. - Growth patterns in fish sagittae, pp. 519-560. In: Skeletal Growth of Aquatic Organisms (Rhoads D.C. & R.A. Lutz, eds). Plenum Press, New York.
- POPPER A.N. & W.N. TAVOLGA, 1981. - Structure and function of the ear in the marine catfish, *Arius felis*. *J. Comp. Physiol.*, 144: 27-34.
- ROSS M.D., POTE K.G., RAREY K.E. & L.M. VERNA, 1981. - Microdisc gel electrophoresis in sodium dodecyl sulfate of organic material from rat otoconial complexes. *Ann. N.Y. Acad. Sci.*, 77: 808-819.
- SHARMA S.K., 1989. - Applications of advanced Raman spectroscopic techniques in earth sciences, pp. 513-568. In: Raman Spectroscopy Sixty Years on. (Bist H.D., Durig J.R. & J.F. Sullivan, eds). Elsevier, Amsterdam.
- SCHUIF A., 1981. - Models of acoustic localization, pp. 267-310. In: Hearing and Sound Communication in Fishes (Tavolga W.N., Popper A.N. & R.R. Fay, eds). Springer-Verlag, Berlin.
- SCHULTZE H.P., 1990. - A new Acanthodian from the Pennsylvanian of Utah, U.S.A., and the distribution of otoliths in gnathostomes. *J. Vert. Paleont.*, 10: 49-58.
- SIMKISS K. & K.M. WILBUR, 1989. - Biomineralization: Cell biology and Mineral Deposition. Academic Press, 337 pp.
- STRONG M.B., NEILSON J.D. & J.J. HUNT, 1986. - Aberrant crystallization of pollock (*Pollachius virens*) otoliths. *Can. J. Fish. aquat. Sci.*, 43: 1457-1463.
- URMOS J., SHARMA S.K. & F.T. MACKENZIE, 1991. - Characterizations of some biogenic carbonates with Raman spectroscopy. *Am. Miner.*, 76: 641-646.
- WEISSBUCH I., ADDADI L., LAHAR M. & L. LEISEROWITZ, 1991. - Molecular recognition at crystal interfaces. *Science*, 253: 637-645.
- WILBUR K.M. & A.S.M. SALEUDDIN, 1983. - Shell formation, pp. 235-287. In: The Mollusca, vol. 4, Physiology, Part I. (Saleuddin A.S.M. & K.M. Wilbur, eds). Academic Press.
- WISE S.W., 1970. - Microarchitecture and mode of formation of nacre (mother-of-pearl) in pelecypods, gastropods and cephalopods. *Ecol. Geol.*, 63: 775-797.
- ZHANG Z., 1992. - Relationship of saccular ultrastructure to otolith growth in the teleost *Oreochromis niloticus*. *J. Morphol.*, 21: 1-10.

Reçu le 18.02.1993.

Accepté pour publication le 08.06.1993.